The Thesis Committee for Kashif Naseem
Certifies that this is the approved version of the following thesis:

Fracture to Production Workflow Applied to Proppant Permeability Damage Effects in Unconventional Reservoirs

APPROVED BY
SUPERVISING COMMITTEE:

Supervisor:

Jon Olson.

Maša Prodanović

Fracture to Production Workflow Applied to Proppant Permeability Damage Effects in Unconventional Reservoirs

by

Kashif Naseem, B.S.

Thesis

Presented to the Faculty of the Graduate School of

The University of Texas at Austin

in Partial Fulfillment

of the Requirements

for the Degree of

Master of Science in Engineering

The University of Texas at Austin

May 2014

Dedication

To my Late Grandma, who was both a father and mother to me and gave me the best advice, support and upbringing that anyone could ask for.

Acknowledgements

I would first thank Allah SWT for without his will, the completion of this thesis would not have been possible. Among humans, I am most grateful to Dr.Olson, whose advice, guidance and assistance was fundamental to the progress of my research. I have learned and benefitted from his knowledge and experience. I would especially like to thank him for his friendly and joyful attitude towards his students which made research much more rewarding and enjoyable. It was truly an honor and privilege to work in his research group. I would also like to thank Dr. Masa Prodanovic for reading my thesis and giving her valuable input in improving its quality.

I am also grateful to Fracture Research and Application Consortium in general and Dr. Julia Gale in particular for their help and assistance during my research. I would also thank Dori for taking care of us both professionally and also by occasionally treating us to cookies and cakes.

I would also like to thank Sh. Umar for his words of wisdom and advice that were always a source of inspiration for me, Mujtaba, Farrokh, Abdul, Muneeb, Talha, Naveed, Arfein, Abdullah, Tuaha, Hasan and everyone else in Nueces Mosque and Austin that made my time here memorable and worth spending. Last but not the least, I am grateful to my family for raising me, supporting me and being there for me whenever I needed them.

Abstract

Fracture to Production Workflow Applied to Proppant Permeability Damage Effects in Unconventional Reservoirs

Kashif Naseem, MSE

The University of Texas at Austin, 2014

Supervisor: Jon E. Olson

Most available data from shale production zones tends to point towards the presence of complex hydraulic fracture networks, especially in the Barnett and Marcellus formations. Representing these complex hydraulic fracture networks in reservoir simulators while incorporating the geo-mechanical parameters and fracture apertures is a challenge. In our work we developed a fracture to production simulation workflow using complex hydraulic fracture propagation model and a commercial reservoir simulator. The workflow was applied and validated using geological, stimulation and production data from the Marcellus shale. For validation, we used published data from a 5200 ft. long horizontal well drilled in the lower Marcellus. There were 14 fracturing stages with micro-seismic data and an available production history of 9 months.

Complex hydraulic fractures simulations provided the fracture network geometry and aperture distributions as the output, which were up-scaled to grid block porosity and permeability values and imported into a reservoir model for production simulation and

history match. The approach of using large grid blocks with conductivity adjustment to represent hydraulic fractures in a reservoir simulator which has been employed in this workflow was validated by comparing with published numerical and analytical solutions. Our results for history match were found to be in reasonable agreement with published results. The incorporation of apertures, complexity and geo-mechanics into reservoir models through this workflow reduces uncertainty in reservoir simulation of shale plays and leads to more realistic production forecasting.

The workflow was utilized to study the effect of fracture conductivity damage on production. Homogenous and heterogeneous damage cases were considered. Capillary pressures, determined using empirical relationships and experimental data, were studied using the fracture to production workflow. Assuming homogenous instead of heterogeneous permeability damage in reservoir simulations was shown to have a significant impact on production forecasting, overestimating production by 70% or more over the course of two years. Capillary pressure however was less significant and ignoring capillary pressure in damaged hydraulic fractures led to only 3% difference in production in even the most damaged cases.

Table of Contents

List of Tables

List of Figures

CHAPTER 1 INTRODUCTION

Shale gas has increased in importance in recent years. Growing demand for energy along with latest technological advancements in petroleum engineering has made vast reserves of shale gas accessible. The most important of these advancements has been in the area of directional drilling and the process of hydraulic fracturing, which has helped in making large reserves of oil and gas from ultra-low permeability formations accessible to operators. Hydraulic fracturing is used to create high permeability pathways in low permeability reservoirs to facilitate the flow of hydrocarbons into the wellbore.

1.1 TYPES OF HYDRAULIC FRACTURES

Hydraulic Fracturing is the creation of cracks or fractures in the subsurface by pumping fracturing fluid into the borehole at a pressure greater than the least stress in the subsurface. The crack that is formed due to rock failure from fluid pressure propagates in a direction perpendicular to the axis of the least stress (Hubbert et al. 1957). Warpinski et al. (2008) classifies hydraulic fractures into four types:

1) Simple bi-wing
2) Complex Fracture
3) Complex Fracture with fissure openings
4) Complex Fracture network

Hydraulic fractures in conventional reservoirs are mostly simple bi-wing structures fractures extending equally on both sides of the borehole (Figure 1.1). These types of fractures are relatively easier to model because of their simple geometry.

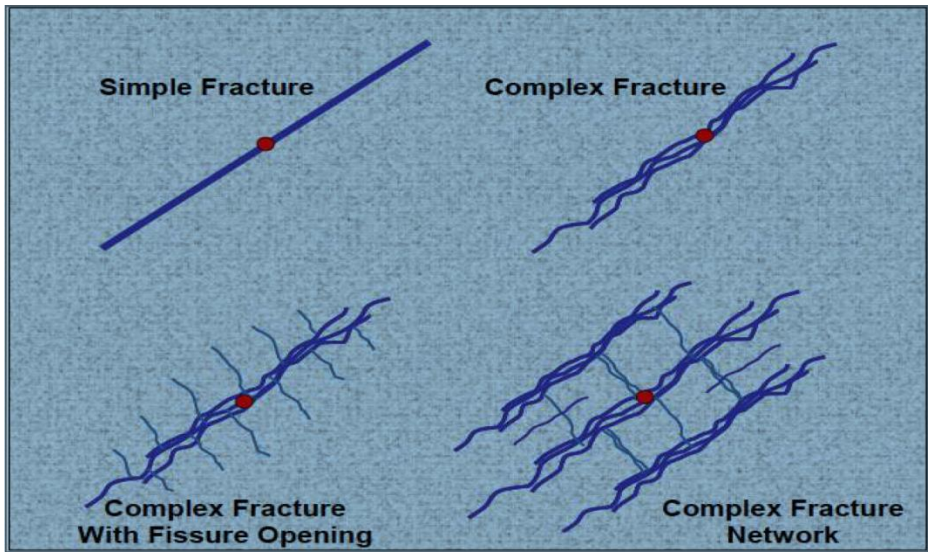

Figure 1.1: Types of Hydraulic Fracture networks (from Warpinski et al. 2008).

1.2 REPRESENTATION OF COMPLEX HYDRAULIC FRACTURE NETWORKS IN RESERVOIR SIMULATORS

The assumption of simple, bi-wing hydraulic fractures might be somewhat accurate in conventional reservoirs, hydraulic fractures in shale usually do not behave in this way. In Barnett shale, fracture growth was shown to be complex through analysis of micro-seismic data (Fisher et al. 2002). Hydraulic fracture networks in Marcellus have also been diagnosed to be complex (Mayerhofer et al.2011). This is primarily due to the presence of natural fractures in shale. The interaction between existing natural fractures and propagating hydraulic fractures leads to change in the direction of propagation for the

hydraulic fracture as well as reactivation of natural fractures leading to complexity (Gale et al. 2007).

Although it is now understood that hydraulic fracture networks in shale are mostly complex due to heterogeneity and presence of natural fractures, representation of this complexity in reservoir simulations has been a challenge. Additionally, incorporating fracture apertures based on geo-mechanics of the area has also not been easy.

Several approaches have been presented to accurately account for the complexity of hydraulic fracture networks in reservoir models. The most common approach is to represent the hydraulic fractures with an orthogonal network of primary and secondary hydraulic fracture networks (Mayerhofer et al. 2006). This model consists of primary hydraulic wings perpendicular to the horizontal well bore, representing the main hydraulic fractures similar to those present in the basic bi-wing model. However, it also includes secondary hydraulic fractures oriented parallel to the wellbore that intersect the primary hydraulic fractures orthogonally. The primary hydraulic fractures are always propped whereas the secondary hydraulic fractures may or may not be propped.

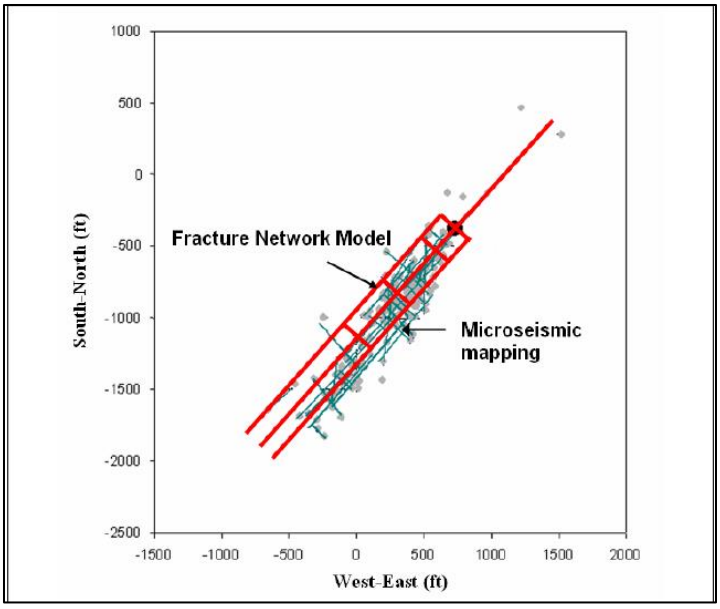

Figure 1.2: Hydraulic fractures represented as an orthogonal network of primary and secondary fractures (from Mayerhofer et al. 2006).

This method of representing fracture complexity does not take into account the prevailing geo-mechanics in the reservoir and only partially accounts for the presence of natural fractures.

Some efforts have been made to couple reservoir simulation with geo-mechanical models. Settari et al. (1998) developed coupled reservoir and geo-mechanical workflows. These workflows were further improved to allow prediction of the Stimulated Reservoir Volume based fracturing job and rock mechanics parameters (Nassir et al. 2014). (Bostron et al. (2009) linked the geo-mechanical simulator Abaqus with Eclipse reservoir simulator through a set of Python scripts. These couplings however were more targeted at accounting for subsidence, overburden effects, compaction etc. Dean et al. (2008) developed a fully coupled geo-mechanical reservoir simulator which accounted for geo-

mechanical parameters in fracture propagation. While this coupling may be able to incorporate fracture apertures into the reservoir model, it is not however, able to depict hydraulic fracture complexity.

Recently, some new models have been developed to represent a complex hydraulic fracture network such as Unconventional Fracture model (Weng et al. 2011) and Wire Mesh (Xu et al. 2010). Some studies have been conducted to establish a workflow from stimulation to production using UFM where UFM is used to model complex hydraulic fracture networks and an unstructured grid model is then used to represent the network in terms of tartan grid cells whose size is small close to the fracture but increases logarithmically as distance from fracture increases. This grid is then used by a production simulator (in this case Schlumberger's INTERSECT) to simulate production (Mirzaei et al. 2012). This workflow is based on the work done by Cohen et al. (2012) where they have coupled the UFM model with a production model. This model is still under development.

Olson (2008) applied a pseudo-3D displacement discontinuity model to simulate the development of a complex hydraulic fracture pattern. The model was originally developed to analyze natural fracture development. It takes into account geo-mechanical parameters like in-situ stresses, mechanical properties of the rock etc. alongside the interaction between hydraulic and natural fractures. It doesn't account for fluid flow in the fractures and instead assumes a constant pressure boundary condition for all fracture branches. This model is called JOINTS and will be referred to by this name from here on in this thesis. Wu (2013) proposed a Fracture Propagation Model (FPM) to model

hydraulic fracture propagation. The model utilizes Displacement Discontinuity Method (DDM) to describe fracture geometry and can predict fracture complexity. It also accounts for fluid flow and pressure drop within the fractures alongside geo-mechanics.

1.3 RESIDUAL GEL DAMAGE

The fracturing fluid should be viscous enough to carry the proppant. This is achieved by adding polymers, the most common of which is guar gum, a natural product extracted from guar beans. After the fracturing process, the fracturing fluid should be removed completely from the fractures in order to allow for the hydrocarbon to flow through. Hence, the polymers are designed to break down under the influence of temperature or additives. However, the broken down polymers might not be soluble in water, e.g. degraded guar gum is not completely soluble in water and leaves a residue (Coke 1975). Studies conducted on the effects of these residues on proppant conductivity have indicated that these broken down polymer gels can lead to a reduction in fracture conductivity (Coke 1975 and Almond et al. 1984). The reduction in conductivity is because of two mechanisms. The first is due to the formation of a gel cake on the walls of the fracture which leads to a reduction in the flow area available and hence reduces conductivity. The second mechanism is due to the reduction of the actual permeability of the proppant pack (Barree 2003). This reduction is caused by plugging of pore throats and pore space in the proppant pack (Palisch et al. 2007).

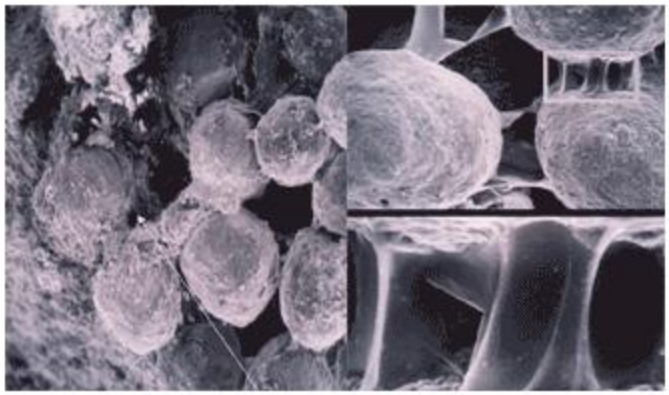

Figure 1.3: Fracture fluid damage in proppant packs (from Carbo Ceramics).

According to Barree (2003), gel damage alone can cause conductivity reduction of anywhere between 20% up to 1000% and in extreme cases, it can completely eliminate conductivity. Engineers typically assign a 50% value to the permeability damage due to gel residue for designing purposes (Palisch et al. 2007). Wang et al. (2009) simulated gel damage in fractures using a 3D, three phase reservoir simulator and found that reduction in gas flow due to damage will be higher in low conductivity fractures than higher conductivity fractures. They also determined that high fracture conductivity is a requirement for effective gel clean up. Wang et al. (2012) used an analytical model to investigate the effects of several formation damage mechanisms on well productivity including gel damage.

Heterogeneous vs. Homogenous Damage

Gel damage is mostly assumed to be homogenous throughout the fracture network in the industry and literature while running reservoir simulations since the distribution of damage in the fracture network is hard to evaluate (Wang et al. 2012). Shale reservoirs

are highly heterogeneous and hydraulic fracture networks created as a result of fracture treatments are quite complex, thus there is high variation in fracture properties such as width, geometry, pressure distribution and even in stress state depending upon the orientation of fracture with respect to the horizontal stresses. Gel damage is primarily dependent upon the pressure in hydraulic fractures and fracture conductivity (Wang et al. 2008) therefore it's likely that gel damage in the fracture networks would be heterogeneous rather than homogenous. Wang et al. (2008) used a 3-D, three-phase black oil reservoir simulator to model gel damage however, they did not account for fracture complexity or aperture changes, and hence the heterogeneity of the gel damage distribution was solely based on the variation in yield stress for the fracturing fluid. Charoenwongsa et al. (2012) incorporated a flow model into their geo-mechanical model coupled with a reservoir simulator in order to account for damage due to fracturing fluid in hydraulic fractures. The model takes fracture aperture into account - however, it can only simulate gel filter cake damage on the fracture face and does not account for the residual gel damage within the fractures. Like Wang et al. (2009), it does not consider fracture complexity.

Capillary Pressure

Due to the high permeability in the proppant pack, the capillary pressure is assumed to be negligible, given that capillary pressure has an inverse square relationship with permeability (Cheng 2012). While this assumption might be appropriate in non-damaged proppant packs where permeability is in the darcies, if the proppant pack is damaged due to gel residue, the permeability of the proppant pack will be reduced to tens

of millidarcies or even less if the damage is severe. Thus, a proppant pack which would have negligible capillary pressure when undamaged might have some capillary pressure after it is damaged by gel residue due to plugging of its pores and resulting reduction in permeability. Currently, this phenomenon has not been acknowledged or investigated in the literature. All works and studies cited above assume capillary pressure in fractures to be zero even if the damage is severe.

1.4 PROBLEM STATEMENT

Most available data suggests well stimulation creates complex hydraulic fracture networks in shale formations such as the Barnett and Marcellus. Representing these complex hydraulic fracture networks in reservoir simulators, including heterogeneous fracture aperture distributions, could have a measurable impact on resultant production. In our work we focused on two broad objectives:

1) Develop a fracture to production simulation workflow using JOINTS and the Schlumberger's Eclipse reservoir simulator, then apply and validate it using geological, stimulation and production data from Marcellus shale.
2) Use the workflow to analyze and investigate residual gel damage in hydraulic fracture networks, specifically:
    i) Effects of heterogeneous vs. homogenous gel damage in hydraulic fractures taking into account fracture complexity and apertures.
    ii) Capillary pressure arising in damaged hydraulic fractures

CHAPTER 2 WORKFLOW and VALIDATION

To develop a practical fracture to production workflow, we used JOINTS, a complex hydraulic fracture propagation model simulator and ECLIPSE, a commercial reservoir simulator. EXCEL, a spreadsheet program was used to receive output from JOINTS, upscale it and transfer it to ECLIPSE to be used in the reservoir model (Figure 2.1). ECLIPSE (E100) (Eclipse) from Schlumberger is a black oil reservoir simulator that utilizes finite volume method to solve material and energy balance equations. E100 does not incorporate geo-mechanics into the reservoir model. JOINTS is pseudo-3D displacement discontinuity fracture propagation software that can simulate crack propagation providing crack geometry and apertures (Olson 2008). It can be used to simulate both natural and hydraulic fractures. For hydraulic fractures, the fluid pressure inside the hydraulic fracture is assumed to be constant throughout the simulation and fractures are fully penetrating with propagation ending at the boundary of the model.

In order to validate the suggested JOINTS to reservoir simulation workflow, it was decided to analyze a case from Marcellus Shale chosen after thorough literature search. The data set in question was from Ajayi et al. (2011). The authors of the paper had used data from this particular well to analyze and evaluate the applicability of channel fracturing techniques in Marcellus Shale. In channel fracturing, stable channels are created and fluids, instead of flowing through a proppant pack, flow through these

channels effectively decoupling fracture conductivity from proppant pack permeability. The data set was fairly complete and included micro seismic data alongside reservoir properties and production history.

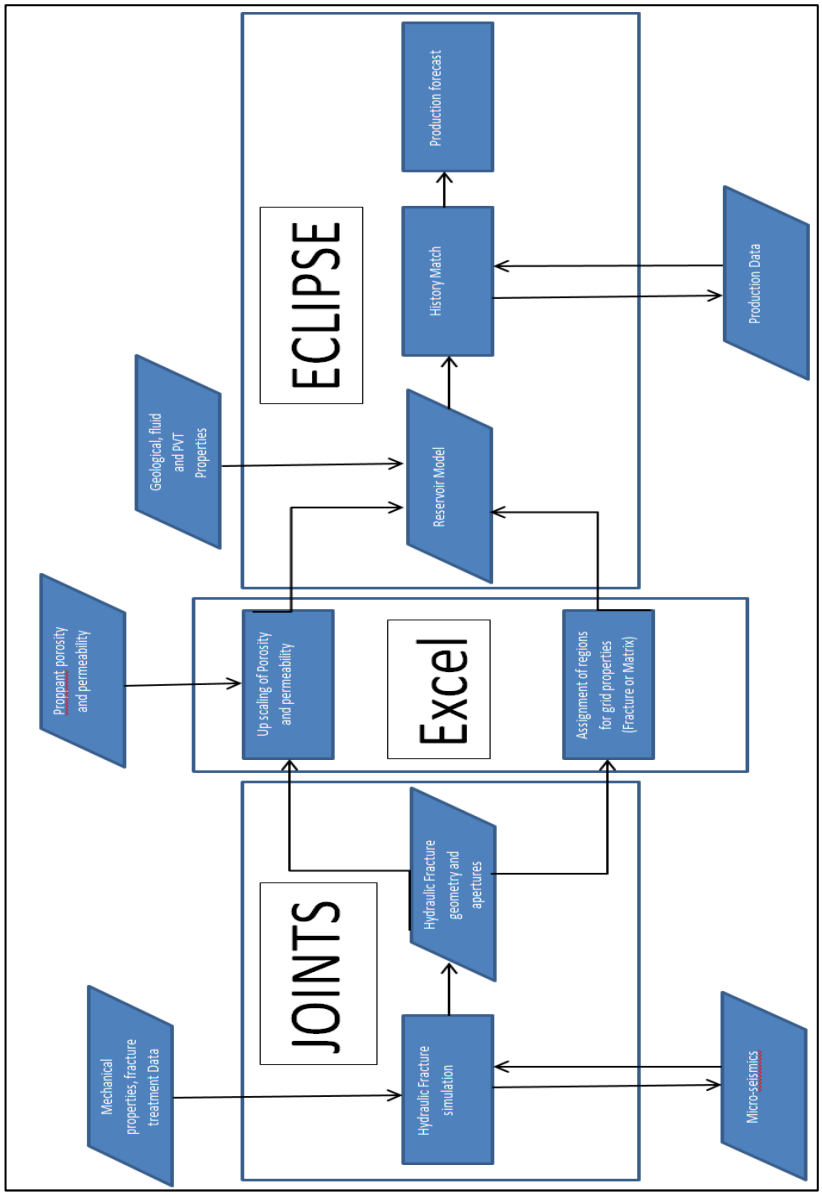

Figure 2.1: Graphical representation of the workflow.

2.1 Representing Hydraulic Fractures in a Reservoir Simulation Model

A variety of approaches have been used to represent hydraulic fractures in commercial reservoir simulators. These include both single and dual porosity approaches. In single porosity approach, the fracture is explicitly represented by individual grid cells in a single plane (Cipolla et al. 2009). In dual porosity modeling, the reservoir consists of two systems, the fracture system to represent natural fractures and fracture networks resulting from hydraulic fracture treatments and the matrix system (Zhang et al. 2009). Within the single porosity models, different methods exist for representing hydraulic fracture cells. One way is through a local grid refinement where grid cells with fractures are further refined with the introduction of narrower cells locally to represent hydraulic fractures. The size and properties of these narrow cells are comparable to an actual hydraulic fracture, and thus enable more accurate modeling of fracture parameters. Another way is through a uniform grid where all grid cells including the ones representing the hydraulic fracture of same size. The permeability and porosity of the fractured grid cells are adjusted to obtain an appropriate conductivity (Li et al. 2011).

Since the output from JOINTS is in the form of uniform grid cells of equal sizes with hydraulic fractures represented by cells of high permeability, we decided to create a reservoir model with the uniform size grid approach. The size of each cell was the same as the size of each element in the JOINTS model - 6.56 ft. x 6.56 ft.

Li et al. (2011) ran simple simulation models varying fracture cell width from 0.1 ft. to 10 ft. and showed that the hydraulic fracture cell size does not impact the simulation results provided that the porosity and permeability are adjusted to obtain the same values

of pore volume and conductivity. However, their work consisted of parameter sensitivity analysis and did not validate the simulation results through analytical solutions or observed data. In this particular workflow, it was decided to validate the results obtained when using a fracture cell width of 6.56 ft., against analytical solutions. The cell width of 6.56 ft. was chosen in order synchronize ECLIPSE with JOINTS since the length of an element in JOINTS was set at 2m or 6.56 ft.

Wattenburger's Method

Two analytical approaches were employed for model validation – Wattenburger's method and Fcd curves of Agarwal. Wattenburger et al. (1998) published the equations for linear flow from a well with a single bi-planar hydraulic fracture. The well was placed in the center of a rectangular area with a bi-planer hydraulic fracture parallel to the shorter side, extending all the way to the boundary. Wattenburger's analytical solutions are derived for linear flow and infinite conductivity fractures but according to Wattenburger, they are applicable for dimensionless conductivities greater than 50. Dimensionless Conductivity (Fcd) is defined as

$$F_{CD} = \frac{k_f w_f}{k_m x_f} \tag{2.1}$$

where

k_f = hydraulic fracture permeability

k_m= matrix permeability

w_f= fracture width

x_f= fracture half length

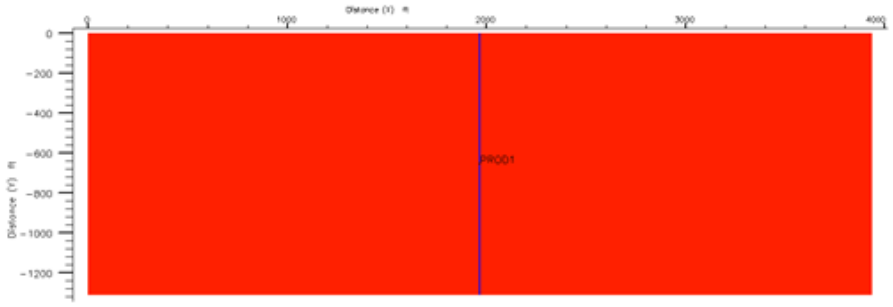

Figure 2.2: Reservoir model used for Wattenburger's Method.

For our simulations, we used an Fcd of 500 which is a common number for dimensionless fracture conductivity in shale formations. Other simulation data are given in Table 2.1. Gas production was simulated for the first 72 months of production at constant wellbore pressure. Inverse production rate (1/q) was plotted against time on a log-log plot (Figure 2.3). The linear flow period of the production manifests itself on the plot after day 1 with a straight line with slope of ½ on log-log plot.

P_i (psi)	8800
P_{wf} (psi)	1600
$m(P_i)$ (psi^2·cp)	2.67E+09
$m(P_{wf})$ (psi^2·cp)	1.67E+08
Mi(cp)	0.0376
Ct (psi^{-1})	8.53E-05
H (ft.)	75
φ	0.1
T (R)	660
S_w	15%
$k_{fracture}$ (mD)	7.6
k_{matrix} (mD)	0.0004

Table 2.1 Reservoir and well parameters used for validation

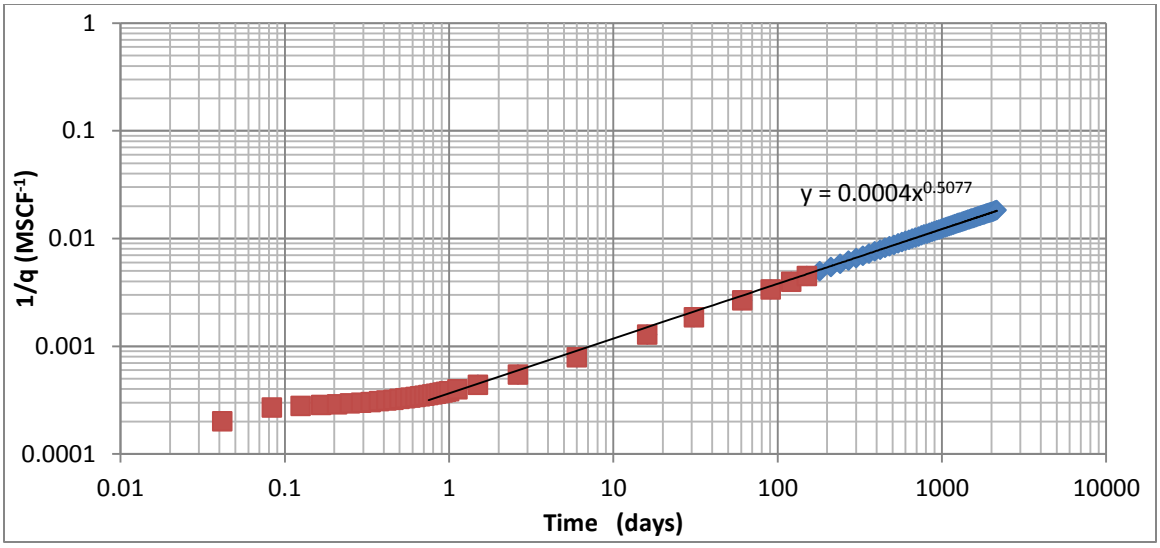

Figure 2.3: Inverse production rate (1/q) plotted against time on a log-log plot.

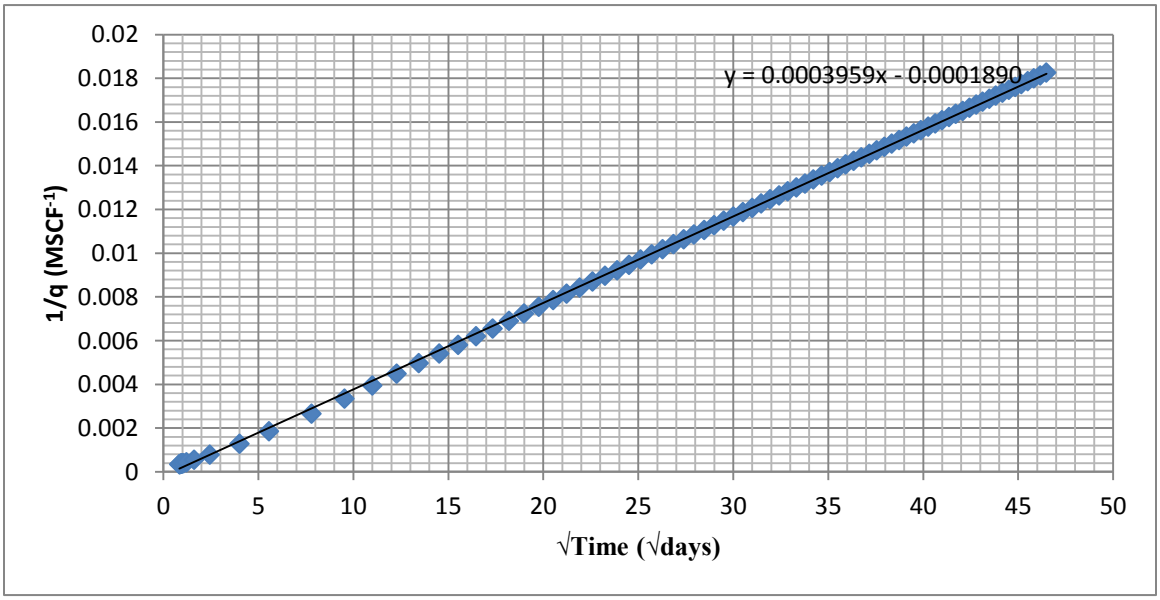

Figure 2.4: 1/q plotted against square root of time.

The linear flow period when plotted on a plot of 1/q vs. √t. (Figure 2.4) gives a straight line whose slope is given by.

$$m = \frac{315.4T}{h\sqrt{\phi(\mu c_t)_i k}\, x_f \Delta m(p)} \tag{2.2}$$

where,

$$\Delta m(p) = m(p_i) - m(p_{wf}) \tag{2.3}$$

h = pay zone thickness (ft.)

μ = viscosity (cp)

k = matrix permeability (mD)

x_f = fracture half length (ft.)

$m(p_i)$ = initial reservoir pseudo-pressure (psi^2/cp)

$m(p_{wf})$ = flowing wellbore pseudo-pressure (psi^2/cp)

c_t = total system compressibility (psi^{-1})

φ = porosity

T = temperature (R)

Thus, the hydraulic fracture half-length can be determined as

$$x_f = \frac{315.4T}{hm\sqrt{\phi(\mu c_t)_i k}\, \Delta m(p)} \tag{2.4}$$

In this case (Fig. 2.4), the xf used in the simulation was 249.3 ft., consistent with the xf = 248.4ft. computed with equation 2.4. We performed additional simulations at different grid sizes ranging from 2 ft. to 50 ft. to evaluate what size was adequate for our problem (Table 2.2). The percentage error does rise as the size of the grid block is increased but all calculated fracture lengths are within 2% error range even in the extreme case where

the grid block size was 50 ft. (Table 2.2). We used a grid block size of 6.56 ft. for our workflow validation and 13.12 ft. for the investigation of gel damage, both of which gave fracture lengths within 1% of the actual length through Wattenburger's analytical solutions.

dx (ft.)	k (mD)	kf (mD)	xf (ft.) (Actual)	Fcd	xf (ft.) (Calculated)	% error
2.00	0.0004	25.00	250.00	500.00	249.81	0.07
5.00	0.0002	5.00	250.00	500.00	249.16	0.34
6.56	0.0004	7.80	249.28	500.00	248.36	0.37
10.00	0.0004	5.00	250.00	500.00	248.61	0.55
25.00	0.0004	2.00	250.00	500.00	247.05	1.18
50.00	0.0008	2.00	250.00	500.00	245.25	1.90

Table 2.2: Actual and calculated fracture half lengths

Agarwal's Approach

Agarwal et al. (1979) provides type curves to analyze pressure transient behavior of low permeability single phase gas wells with finite conductivity fractures in an infinite reservoir. The type curves were created through transformation of simulation results using dimensionless definitions. For constant wellbore flowing pressure, the type curves plot the reciprocal of the dimensionless production rate (q_D) vs. dimensionless time based on fracture half length (t_{Dxf}).

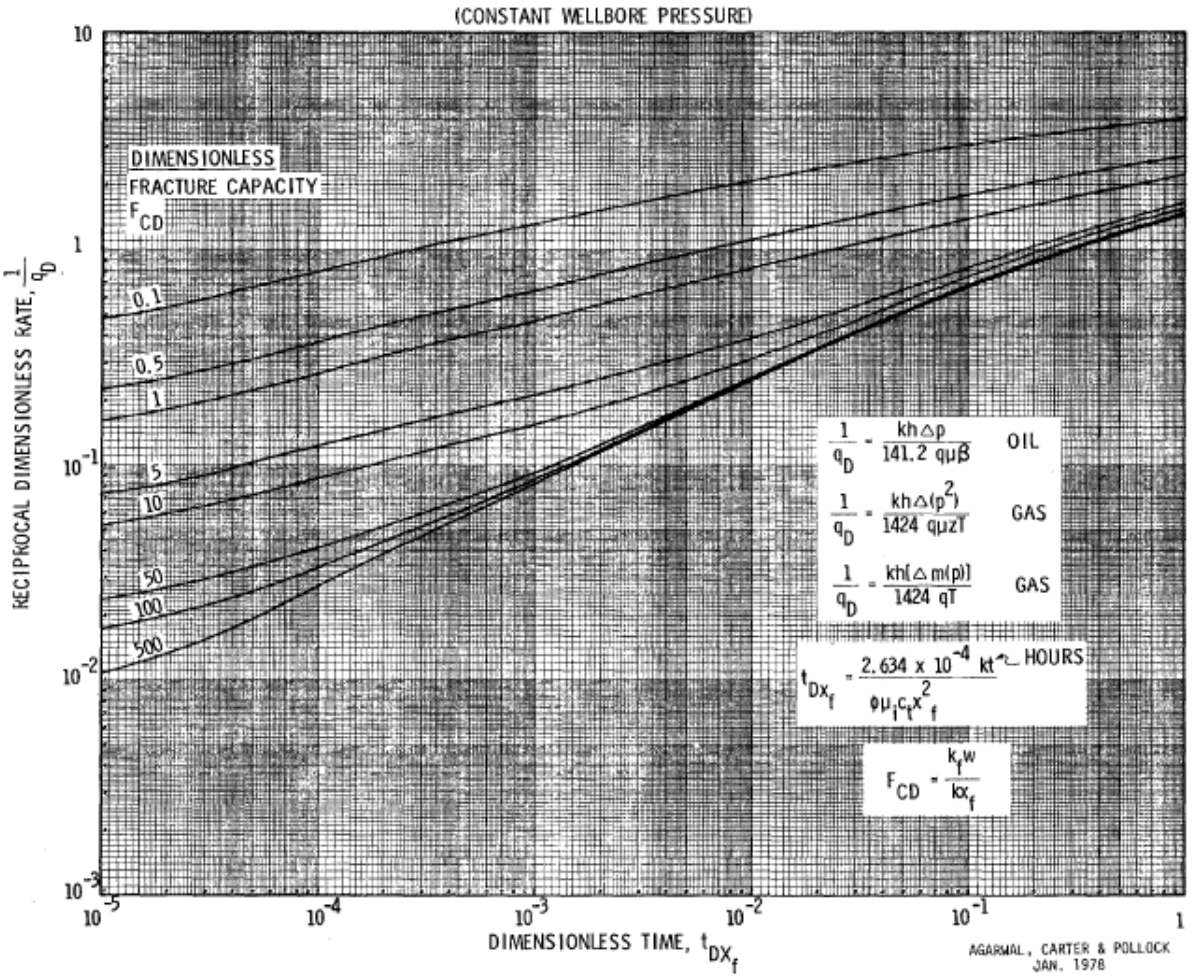

Figure 2.5: Type curves for finite capacity vertical fractures (Agarwal et al. 1979).

The reciprocal of dimensionless production rate is given by

$$\frac{1}{q_D} = \frac{kh\Delta(p^2)}{1424q\mu zT} \tag{2.5}$$

where

$$\Delta p = p_i - p_{wf} \tag{2.6}$$

q = flow rate (MSCF/day)

h = pay zone thickness (ft.)

μ = viscosity (cp)

k = matrix permeability (mD)

c_t = total system compressibility (psi^{-1})

φ = porosity

T = temperature (R)

z = real gas compressibility factor

p_i = initial reservoir pressure (psi)

p_{wf} = wellbore flowing pressure (psi)

t_{Dxf} is calculated is given by

$$t_{Dx_f} = \frac{0.0002634kt}{\phi\mu_i c_t x_f^2} \tag{2.7}$$

where

t = flowing time (hrs.)

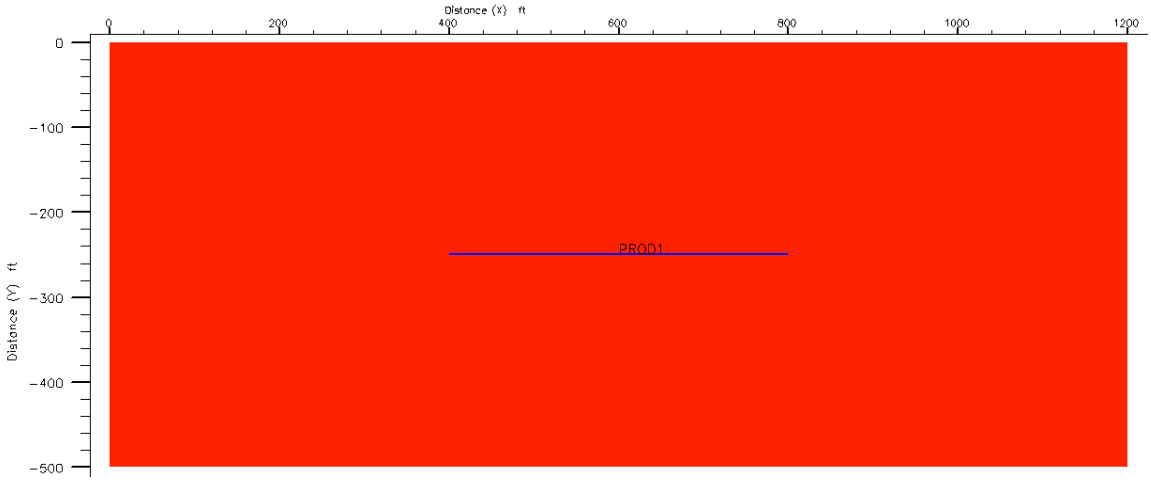

Figure 2.6: Reservoir model used for to plot type curves. The model satisfies the assumption of infinite acting reservoir.

Simulations were run using a reservoir model and properties which satisfied the assumption of infinite acting reservoir required for Agarwal's type curves i.e. flow did not reach pseudo steady state in any of the simulation cases till the end (Figure 2.6). Production results were converted into dimensionless form using Equation 2.4 and 2.6 and type cures were then plotted for Fcd of 5 and 500 for a range of fracture grid cell sizes. The dimensionless results were compared between Agarwal et al. (1978) and our model (Figure 2.7 and 2.8). For both conductivities, it can be seen that curves obtained from our data do not match with Agarwal's type curves in the early time. The time duration for which the curves do not match depends on the size of the grid block but for the grid cell size range of 2ft – 20 ft. which is realistically what will be used in the workflow, this early time ranges from 0-3 months. Hence it can be said that using grid block sizes on the order of feet to represent hydraulic fractures that have widths on the order of fractions of inches does not introduce substantial error beyond the first 2-3 months of production provided the fracture grid block size does not exceed 20 ft.

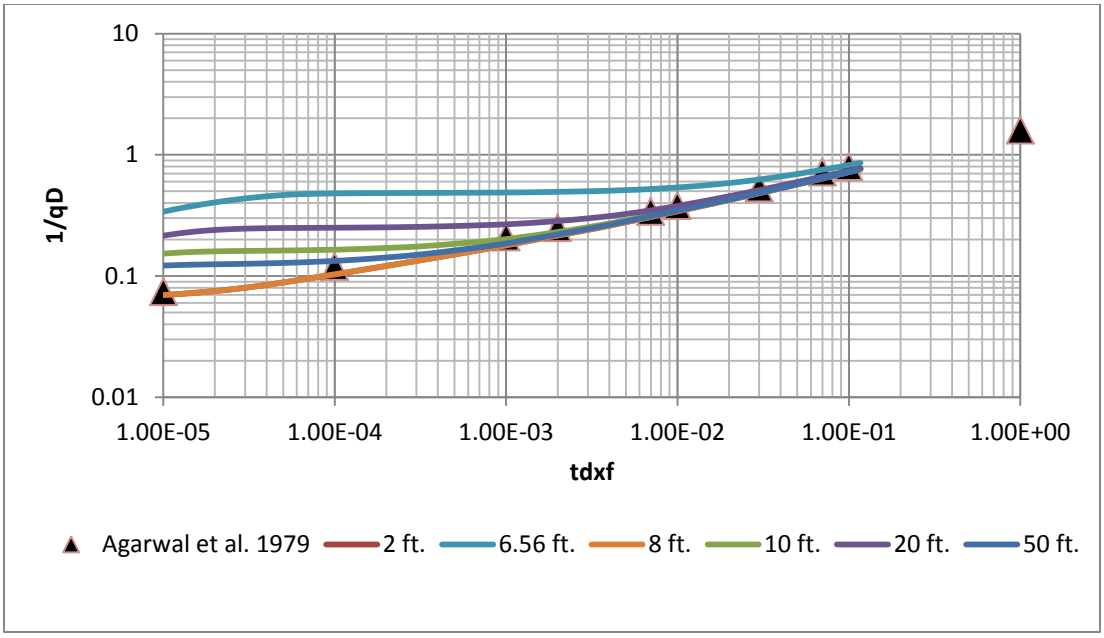

Figure 2.7: Type curves for Fcd=5.

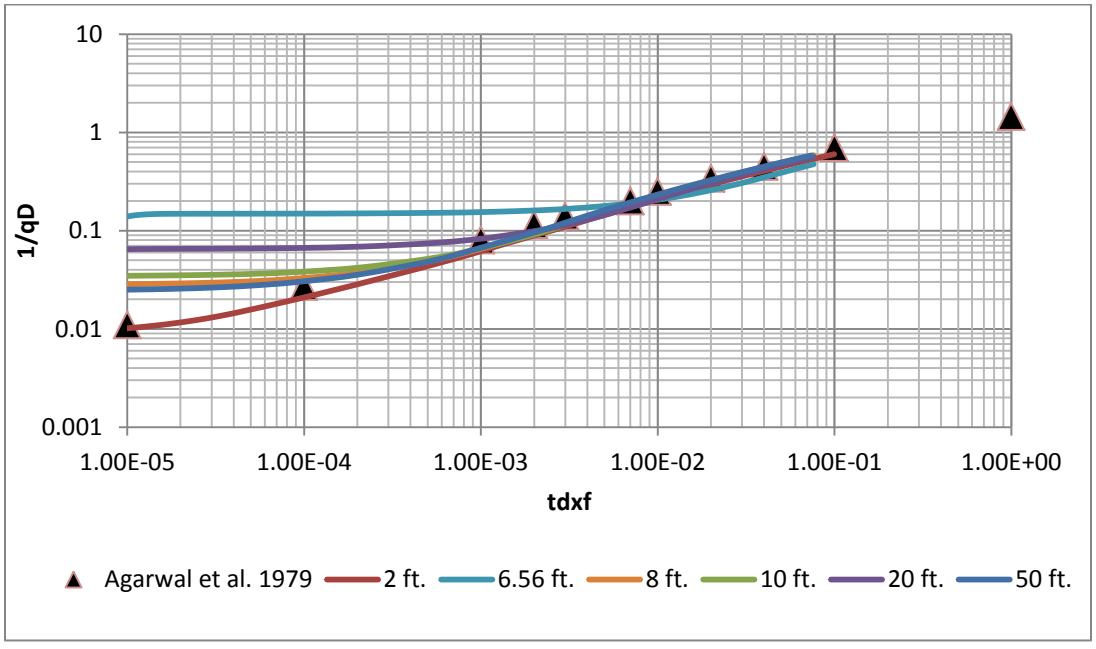

Figure 2.8: Figure 2.7 Type curves for Fcd=500 showing better agreement between type curves in the late time.

2.2 MODELING NATURAL FRACTURES IN MARCELLUS SHALE

To successfully simulate a complex hydraulic fracture network, it is essential to have information about natural fracture spacing, orientation and pattern in a shale formation, alongside the mechanical properties of the rock. There are three dominant natural fracture sets in Marcellus Shale (Engelder 2009). The J1 set, which strikes NE-SW, is older and is parallel to the current S_{Hmax} direction. The second set is J2, which is roughly perpendicular to J1, although the orientations of J2 are not very consistent. The third fracture set (J3) is nearly parallel to J1. In the Marcellus, interaction between natural and hydraulic fractures can cause slip in both J1 and J2, activating both fracture planes and producing a very complex hydraulic fracture network (Stroud et al. 2012). The fractures are contained by the underlying Onondaga formation and the Tully Limestone on top. Both of these formations have stress gradients on the order of 1 psi/ft., compared to 0.8-0.9 psi/ft. in the reservoir layers hence they act to inhibit fracture height growth.

In order to characterize natural fractures in Marcellus, a joint project was undertaken with the Bureau of Economic Geology in UT in order to characterize and model natural fractures. Core analysis and outcrop studies were performed by geologists and we carried out JOINTS modeling to simulate the formation of J1 natural fractures. Details of the entire project can be found in Gale et al. (2012). JOINTS (Olson et al, 2009) simulates crack propagation by taking mechanical properties of the material as the input (Table 2.3). The user specifies the length and location of starter cracks which are treated as initiation points for fractures. Marcellus rock samples from Washington County, Pennsylvania were analyzed in a lab in order to determine mechanical properties.

Fracture Friction coefficient	0.6
Subcritical index	80
Fracture Toughness	1.3
Poisson's Ratio	0.2
Young's Modulus	20000 MPa
Strain in X direction	0
Strain in Y direction	0.00001
Initial X strain	-0.000002
Initial Y strain	0
Loading Time	1 million years

Table 2.3: Mechanical properties and input parameters used for modeling of natural fractures

The natural fracture propagation simulation was performed over an area of 50 ft. x 200 ft. Since computational time increases dramatically with simulation size, we couldn't model the entire Marcellus reservoir. We chose to make the simulation area longer in the spacing direction to generate more meaningful statistics for that parameter. We restricted the natural fractures to be planar based on field observations. Fracture spacing is the perpendicular distance between fractures. The resulting fracture pattern (Figure 2.5) shows minimal fracture clustering with an average spacing of 4.29 meters.

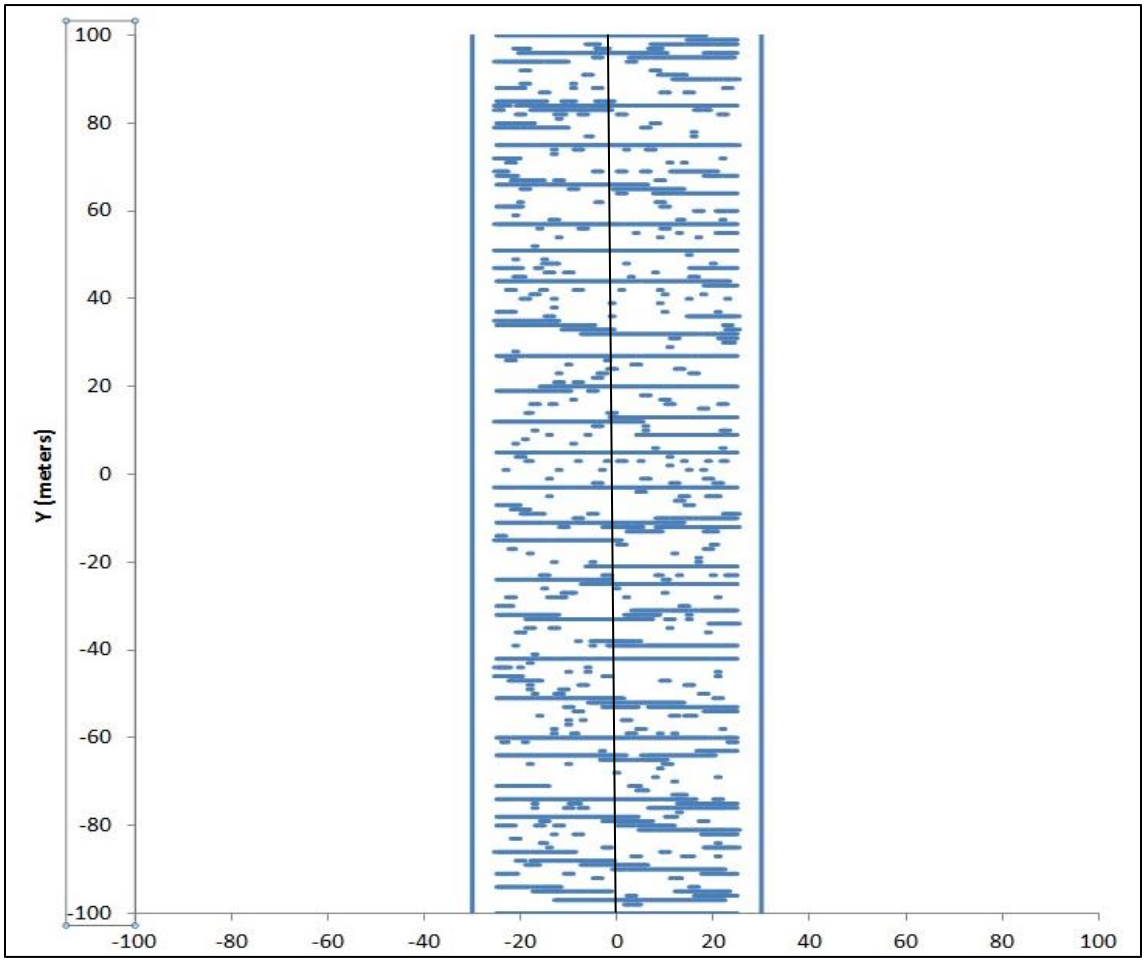

Figure 2.9: Natural Fracture distribution obtained from JOINTS.

JOINTS also generates the aperture data for each time step of the simulation. It was decided to use 1 mm as the threshold value for aperture i.e. any fracture with an aperture less than 1 mm would be ignored and not counted as a fracture. This threshold was required for the ease of comparison with the outcrop data. The scan line used to analyze outcrops is not able to identify very small fractures hence a thresh hold was needed to filter out fractures lower than a particular size when analyzing the model.

A scan line was run to determine the spatial configuration of the fractures. A scan line was run on the model to quantify the clustering in the fracture pattern. It was found that spacing of 9.5 and 20 m were slightly more common in the pattern then they would be in a random distribution of fractures although the preference for this spacing was not very strong.

Analysis of outcrop data showed that spacing of 0.2m, 1m, 7m and 14m were more common in the outcrop. Thus the fractures in the outcrop are closer than determined from outcrop which is acceptable since fractures are usually more closely spaced in outcrops then in the subsurface as they contain additional fractures formed due to weathering and uplifting, not necessarily present in the original fracture pattern in the subsurface (Marrett 2007). Thus for J1, it was decided to use the spatial configuration determined from 50 ft. by 200 ft. model as it is, repeated over the entire length of the reservoir. Modeling was not possible for J2 since that would require prior insertion of existing J1 fractures into the model prior to the simulation which is not possible with JOINTS at this stage. Field data from outcrop however was available for J2 fractures and showed preferred fractured spacing of 2, 4 and 14m, thus fractures were inserted into the model using this spacing.

2.3 SIMULATING HYDRAULIC FRACTURES

JOINTS cannot model a scenario where a hydraulic fracture intersects a natural fracture and continues propagating without being diverted into the natural fracture. To compensate for this, instead of considering long fractures, fractures of shorter lengths, in the order of 3-5m were inserted. Thus a fracture 20m long would be represented by several small fractures 2m in length with spaces in between. This can geologically be

justified by considering the cementation inside a long fracture. The fracture would be cemented at places making it easier for a propagating hydraulic fracture to cross through without being diverted into the natural fracture. This 'highly cemented' section of the natural fracture is represented by an empty space in JOINTS model. Then there would be other locations in the fracture where it would have weak or no cementation thereby causing the hydraulic fracture to be diverted into the natural fracture. These sections are represented by actual fracture seeds in the model (Figure 2.10).

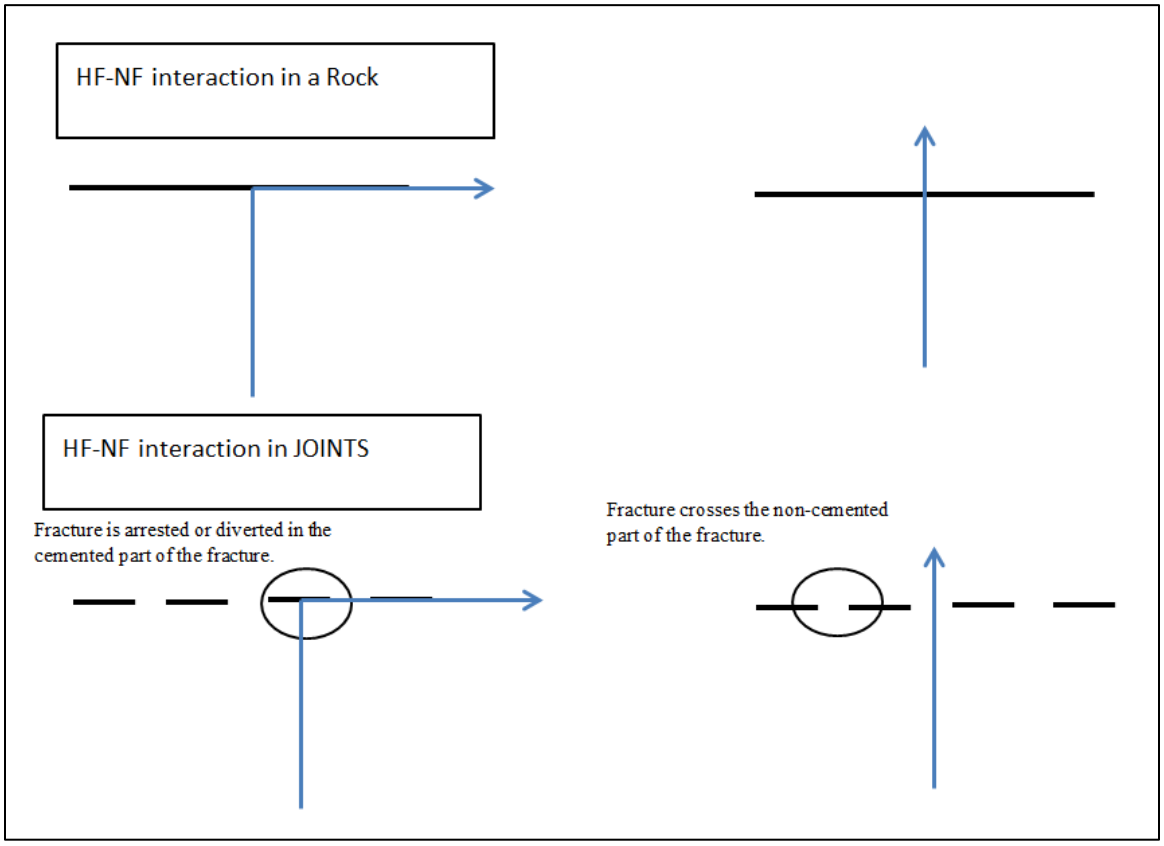

Figure 2.10: Interaction of natural and hydraulic fractures represented in JOINTS.

JOINTS model setup

Based on the observations and data collected in the RPSEA project (Gale et al. 2012), the hydraulic fracturing simulations were performed in a medium with two fractures sets. The J1-analagous set was oriented parallel to S_{Hmax} as indicated by Engelder (2009). The spacing of these fractures was derived from the JOINTS simulations conducted earlier. The second set was J2 inserted perpendicular to S_{Hmax}. The spacing between the fracture seeds was derived from outcrop data.

As mentioned before, the data for the validation process was taken from Ajayi et al. (2011). The well was drilled in north-eastern Pennsylvania, and micro-seismic monitoring was used during the hydraulic fracturing process to track the hydraulic fracture geometry. The well had a horizontal length of about 5200 ft. with 14 stages. (Table 2.4). Micro-seismic data was also acquired during the fracturing process and showed relatively longer fracture lengths and larger simulated volume in the first and final fracturing stages as compared to the middle stages. (Figure 2.7)

Length of Lateral	5200 ft.
Number of fracturing stages	14
Formation	Lower Marcellus
Wellbore Radius	0.325 ft.
Thickness of pay zone	165 ft.
Amount of Proppant used	500000 lb./stage

Table 2.4 Completion and Stimulation Parameters for the well

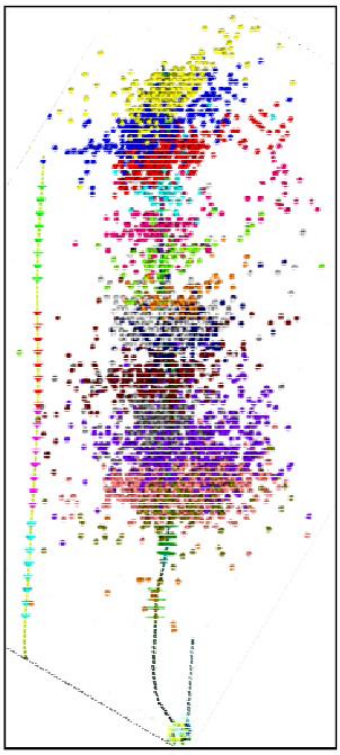

Figure 2.11: Micro-seismic data collected around the well during hydraulic fracturing treatment (from Ajayi et al. 2011).

At this time JOINTS cannot simulate partially penetrating hydraulic fractures. This is because the fluid pressure is constant in the hydraulic fractures all through the simulation and the only forces that vary are geo-mechanical thus the fracture propagation will terminate only after all the cracks have reached the end of the area being modeled, thus the width of the modeled area will also be the width of the stimulated reservoir volume. Hence when choosing an area for fracture propagation, compensation had to be made for that.

In order to choose an appropriate stimulated area, micro seismic data was analyzed. The width of the area to be simulated in JOINTS was determined by assigning

an approximate area to each discrete micro seismic cloud (represented by solid lines on Figure 2.8). Each of these areas was summed and the sum was divided by the stimulated length of the lateral to get an average width of the stimulated region. The resulting area is shown in Figure 2.8 as a bold line. The dimensions of this area are 5904ft x 1050ft.

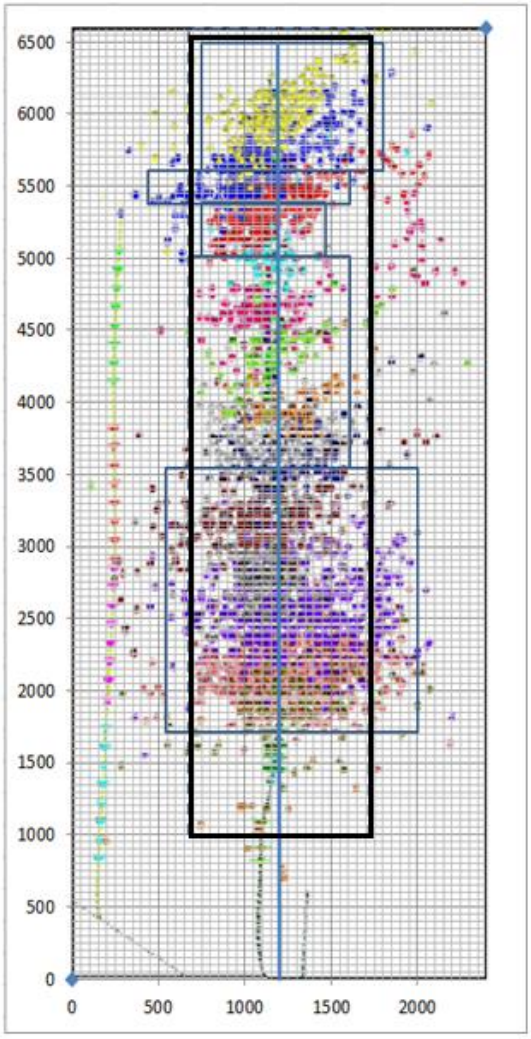

Figure 2.12: Area for JOINTS modeling calculated by averaging regions of micro-seismic cloud over the entire length of the stimulated area.

Horizontal stresses for the data set in Ajayi et al. (2011) were not available hence generic values of horizontal stress gradients for Marcellus derived from Starr (2011) were used to calculate minimum and maximum horizontal stresses (Table 2.5). The model was run in JOINTS and the resulting hydraulic fracture network is provided in Figure 2.13, superimposed over the micro-seismic cloud to give an idea of the location of hydraulic fractures with respect to the micro-seismic. The micro-seismic seem to match with simulated hydraulic fractures for the first and last treatment stages. However, the fracture stages in the middle do not seem to match with micro-seismic at all. This might be due to localized variability in geology and natural fracture distribution which we could not model due to lack of data.

Fracture Friction coefficient	0.6
Subcritical index	20
Fracture Toughness	1.3
Poisson's Ratio	0.2
Young's Modulus	20000 MPa
S_{Hmax}	4500 psi
S_{hmin}	4400 psi
Fluid Pressure in hydraulic fractures	4600 psi
# of Fracture seeds	450

Table 2.5: Mechanical and simulation properties of the formation used for hydraulic fracture simulation

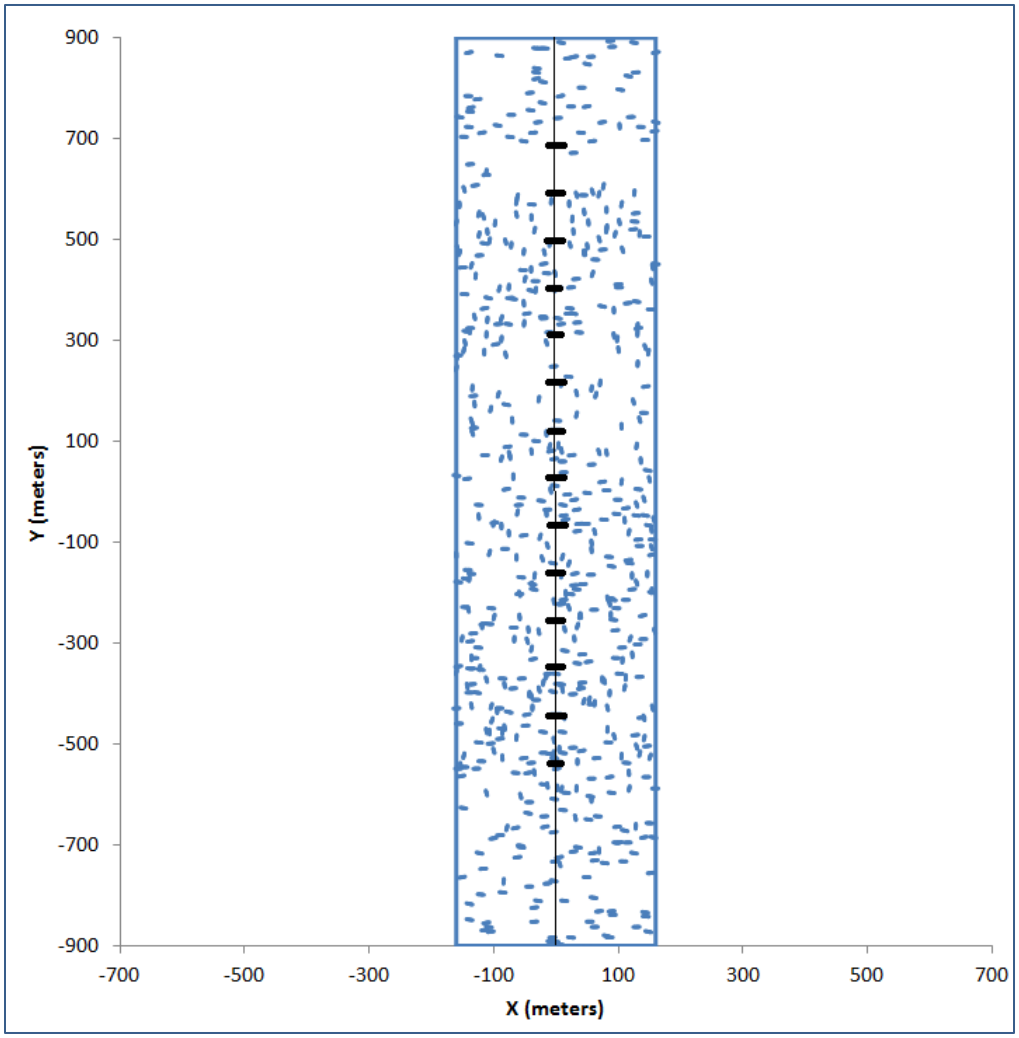

Figure 2.13: Joints model before hydraulic fracture propagation. Fracture stages are marked as well.

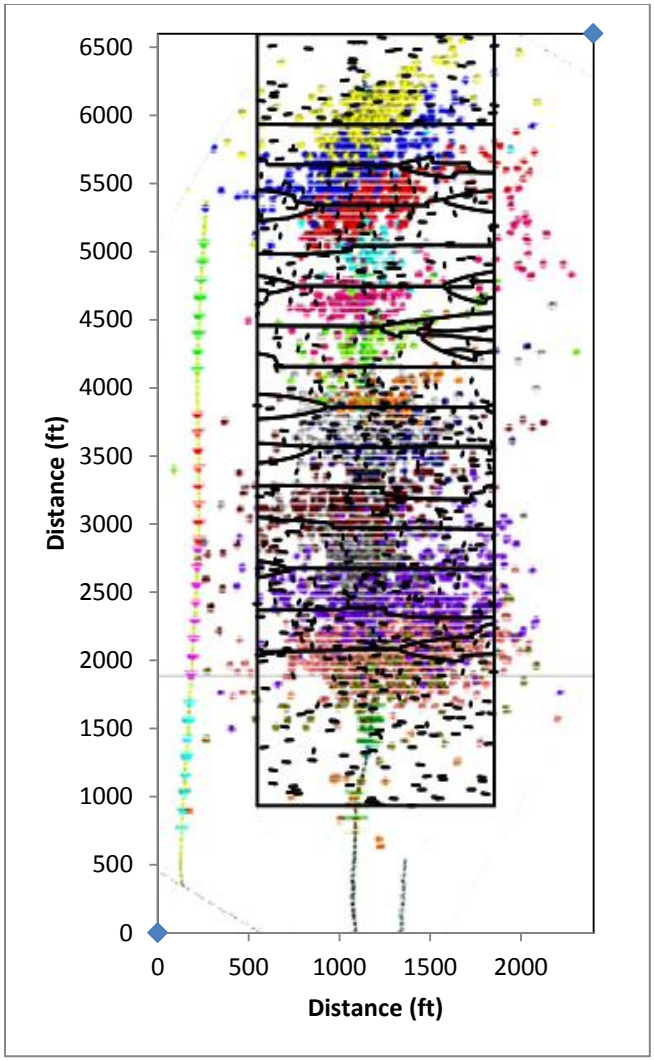

Figure 2.14: Trace map of the hydraulic fracture network obtained from JOINTS, superimposed over the micro-seismic data.

Extracting geometry and apertures

JOINTS can export the fracture geometry of the network by calculating the permeability of every grid block and creating a text file with permeability distribution of the model. Fracture network can be identified as having permeability much higher than the rest of the grid blocks. Actual permeability, though provided by JOINTS is not used

and is only used to identify fracture geometry. JOINTS also calculates the aperture distribution of the fracture network which are used to calculate the conductivity of the fractures.

2.4 RESERVOIR SIMULATION

Assignment of Grid Properties

Once all data had been extracted from JOINTS, it was up scaled in EXCEL. In order to assign permeability and porosity to each fracture grid block, the matrix and proppant properties were scaled according to the dimensions of the fracture grid blocks, so that fracture conductivity is preserved. For permeability,

$$k_{fracture} = \frac{wk_{proppant}}{6.56} \tag{2.7}$$

Likewise for porosity,

$$\Phi_{fracture} = \frac{w\Phi_{proppant}}{6.56} \tag{2.8}$$

Thus, fracture conductivity was preserved during the up scaling. As mentioned before, as long as conductivity does not change, the width assigned to the fracture grid block in the reservoir model will not have any significant effect on the accuracy of the results.

Reservoir Model Properties	
Reservoir Parameters	
Depth (ft.)	7000
Thickness	165
Rock Properties	
Matrix Porosity	3.30%
Rock Compressibility ($Psi^{-1)}$	0.000001
Fracture Porosity	40%
Well Parameters	
Wellbore Diameter (ft.)	0.325
Length of Lateral (ft.)	5200
Initial Condition	
Reservoir Pressure (psi)	4156
Water Saturation	0.15
Fluid Properties	
Standard Pressure (psi)	14.7
Standard Temperature (F)	60
Reference Temperature (F)	130
Grid Properties	
Number of cells in x-direction	900
Number of cells in y-direction	160
Number of cells in z-direction	3
Dimensions of grid block (ft.)	6.56 x 6.56 x 55

Table 2.6 Basic properties of the Reservoir Model

The grid permeability and porosities were then imported into ECLIPSE reservoir simulator (Figure 2.11). The slight variations in permeability within the fracture network are to account for the variability in apertures since the fracture width in the reservoir model is fixed at one grid block. However, the apertures vary over the entire fracture

network with branches closer to the well bore having higher apertures then the ones further away.

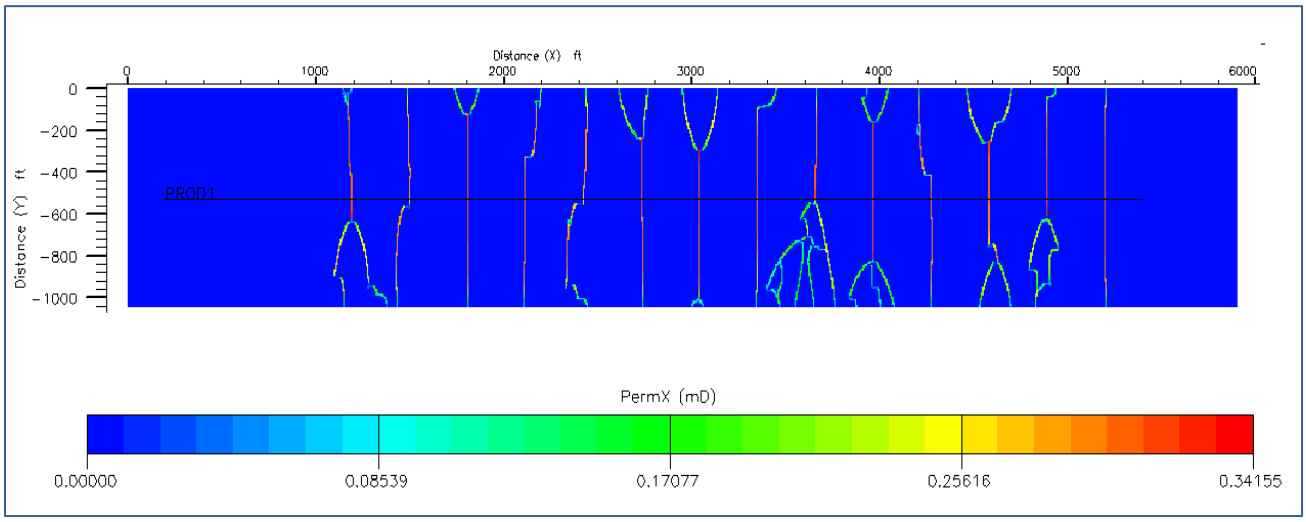

Figure 2.15: Permeability map of the reservoir model in ECLIPSE.

Different fluid and rock properties were assigned for matrix and fracture regions. Capillary pressure and relative permeability curves for shale from Cheng et al. (2012) were used in the reservoir simulations (Figures 2.16, 2.17, 2.18). These are generic curves of the type commonly used in the industry for shale and are quite similar to the curves used for conventional reservoirs. Modeling of relative permeability and capillary pressure curves in shale is a challenging and complex process, due to the composition and ultra-low permeability (Devegowda et al. 2012), thus most of the industry currently uses curves which are in essence, slightly modified versions of the ones used for conventional reservoirs when running reservoir simulations for shale.. Hydraulic fractures have a much higher permeability than the matrix and therefore capillary forces

are considered to be negligible thus the capillary pressure in the hydraulic fractures was assumed to be zero for this case.

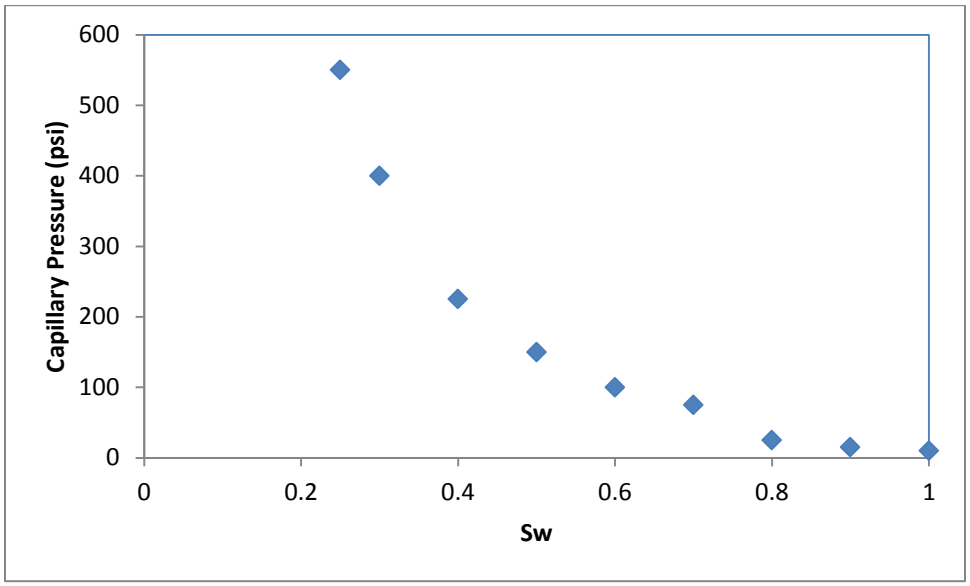

Figure 2.16: Capillary Pressure Curve for Matrix (Cheng et al. 2012).

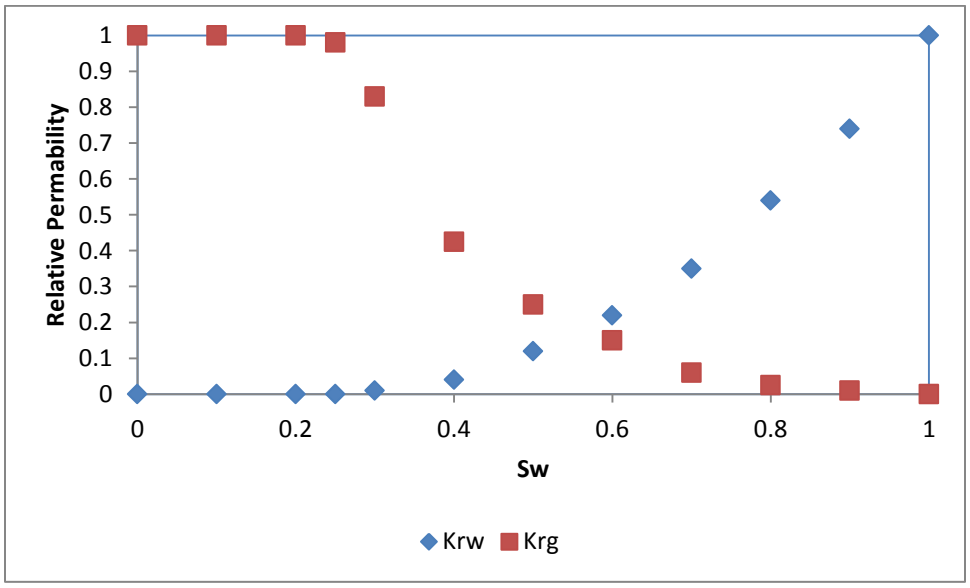

Figure 2.17: Relative Permeability curves for Matrix (Cheng et al. 2012).

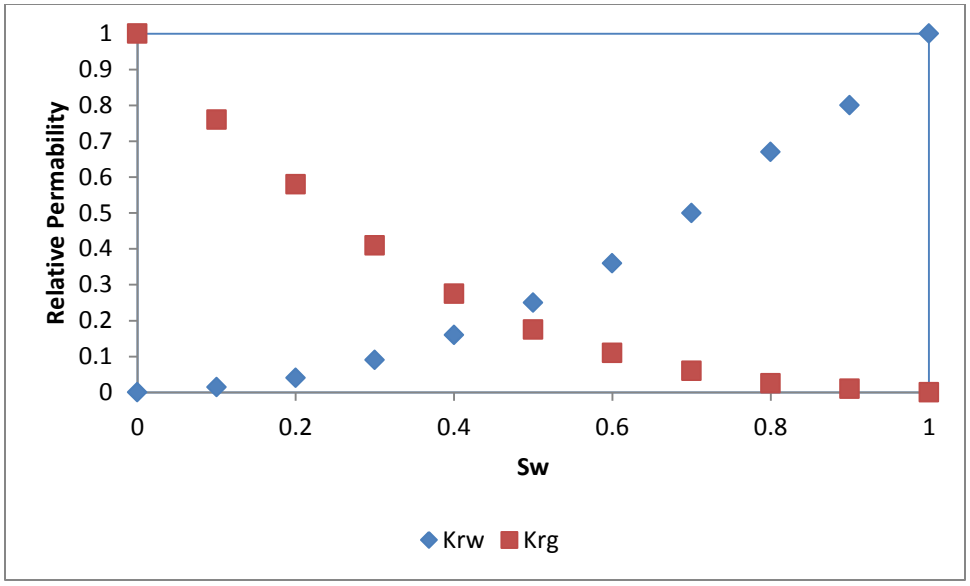

Figure 2.18: Relative Permeability curves for Fractures (Cheng et al. 2012).

There was 9 months of production history available for the well along with the bottom hole pressure data. No fracturing fluid flow back data was available so that process was not simulated. Consequently, initial water saturation in the fractures was the same as in the matrix. The bottom hole pressures were smoothed out and averaged over suitable intervals to eliminate noise (Figure 2.19).

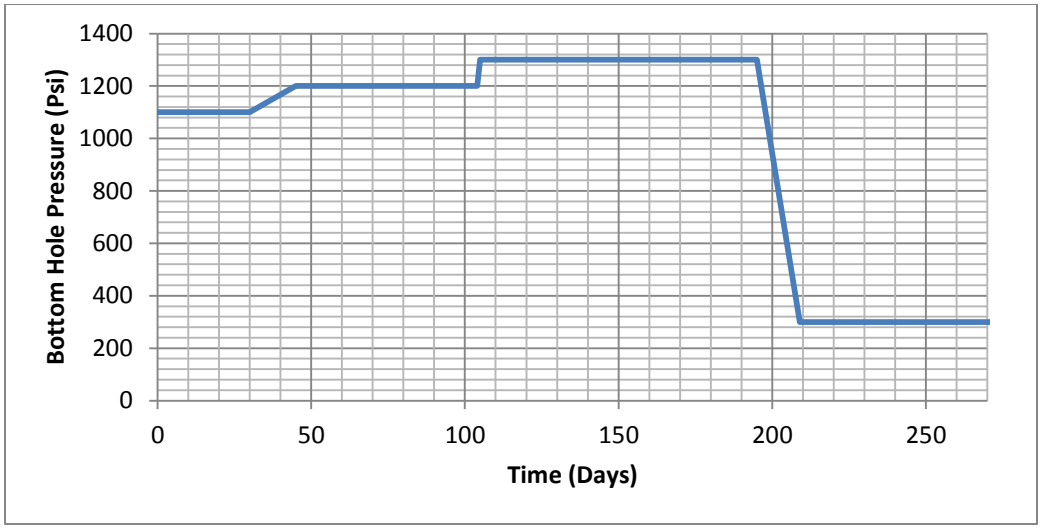

Figure 2.19: Bottom hole pressures for the duration of production.

No petro physical data was available to provide an estimate of the matrix permeability and considering the various damage mechanisms for proppant conductivity such as proppant crushing, gel damage etc., proppant conductivity is also highly variable. Therefore permeability of the matrix and conductivity of the hydraulic fracture were selected to be varied to obtain a production history match. The first simulation run was made with a base case using 100 nD as the matrix permeability and an average fracture conductivity of 22.6 mD-ft. However, the resulting production rate was much higher than the observed production rate in the data set; hence both matrix permeability and fracture conductivity were reduced until a best possible history match was achieved with a matrix permeability of 10 nD and an average fracture conductivity of 2.26 mD-ft. (Table 2.7). For these parameters, the production seemed to be slightly higher than observed gas

production for the first 200 days and lower for the last 70 days of available production data but gave the best match overall (Figure 2.20).

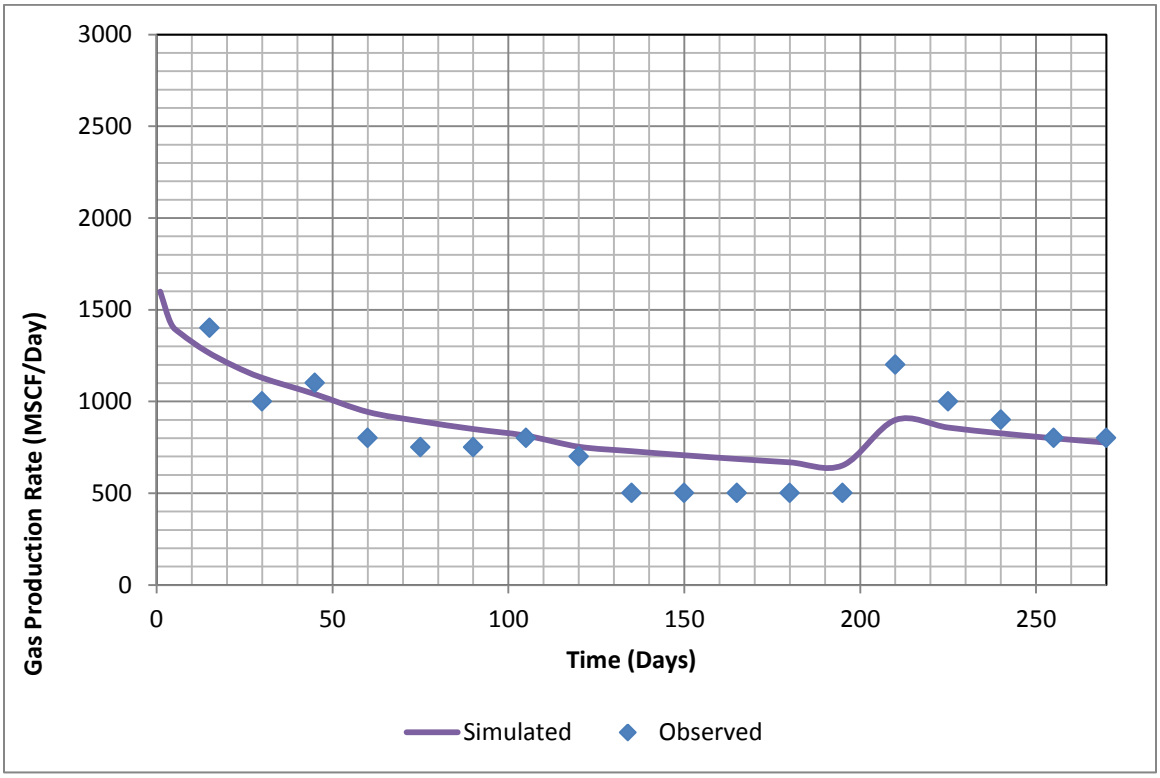

Figure 2.20: Observed and simulated production rates after history match.

Variable Parameters	
Matrix permeability (nD)	10.00
Average Fracture Conductivity (mD-ft.)	2.14
Maximum Fracture Conductivity (mD-ft.)	2.24
Minimum Fracture Conductivity (mD-ft.)	.025

Table 2.7 History Matched Matrix permeability and fracture conductivities.

You should say that the pressure drawdown for this ultra-low perm case (Figure 2.21) shows that there was no interference between the fractures after 9 months. There also seems to be significant pressure drop within the fracture network where parts of the network closer to the wellbore are at a lower pressure then the ones further away. This is expected as fracture conductivity is variable due to the variation in fracture apertures. Fractures are wider closer to the wellbore but the aperture and thus the conductivity decreases further away. (Figure 2.21)

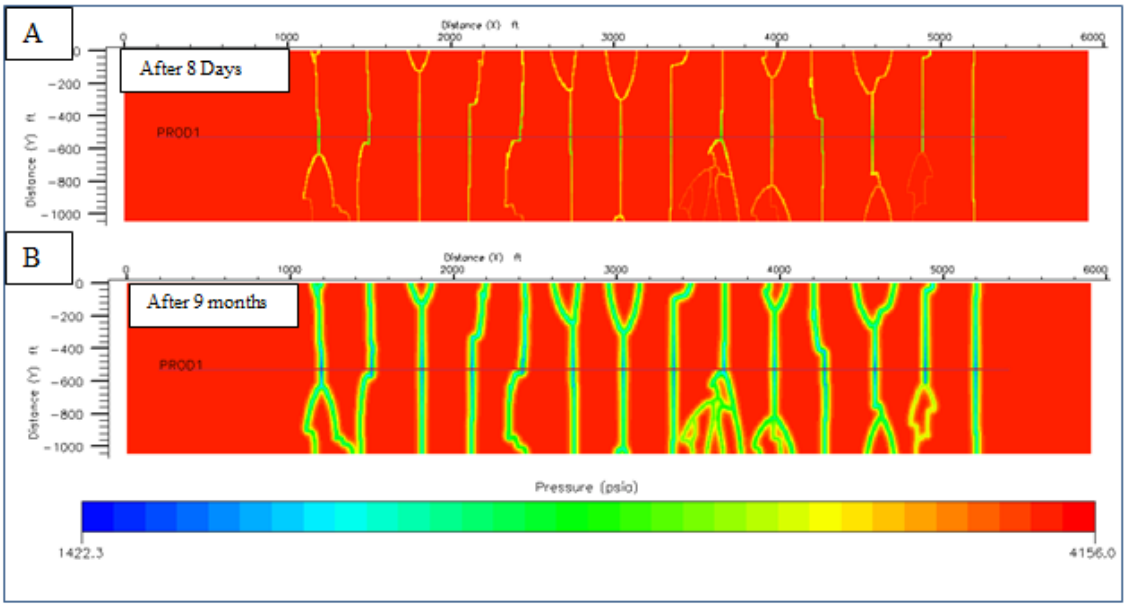

Figure 2.21: Distribution of pressure around the well A) after 8 days and B) after 9 months.

Ajayi et al. (2011) used a matrix permeability of 72 nD and fracture conductivity of 1.3 md-ft. to obtain a history match. Our values of 10 nD and 2.14 mD-ft. were of the same order of magnitude, indicating reasonable agreement between the two simulations

given the uncertainty in many of the parameters. The difference in matrix permeability and fracture conductivity between our model and that of Ajayi et al. can be because of the differences in the way hydraulic fractures were modeled in the reservoir simulation. A combination of these differences provided below, could have led to the higher conductivities and lower matrix permeability determined in our model.

1) The drainage area chosen for the simulation in our case was an average stimulated area selected after averaging all the regions covered by the micro-seismic cloud. Ajayi et al. (2011) however, chose a simulation area such that it covered the full extent of even the largest micro-seismic cloud and thus is larger than ours (Figure 2.22). Thus our area was smaller.
2) Our hydraulic fracture network had some complexity with fractures branching out further away from the wellbore whereas hydraulic fractures in Ajayi et al.'s model were simple bi-planner with varying lengths but no complexity hence our model had a higher effective hydraulic fracture length.
3) Hydraulic fractures in our model had variable apertures and thus variable conductivities whereas hydraulic fractures in Ajayi et al. model had single conductivity value throughout the fractures.

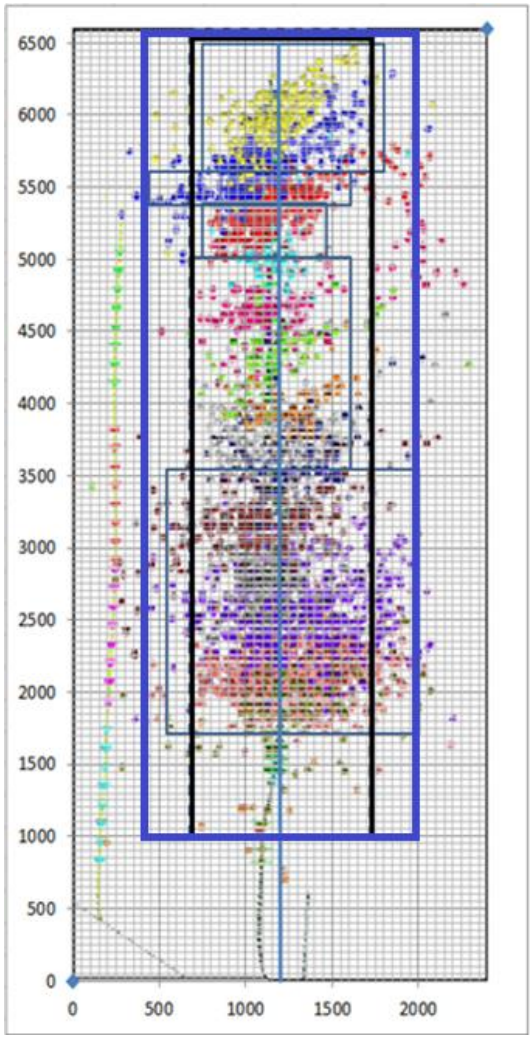

Figure 2.22: Simulation area used by Ajayi et al. (2011) represented by blue outline. Black outline represents our simulation area.

CHAPTER 3 INVESTIGATION OF RESIDUAL GEL DAMAGE: SIMULATION SET UP

The JOINTS to reservoir simulation workflow is not only applicable to production forecasting but can also be used to investigate other problems and hypothesis related to reservoir simulation of hydrocarbon production in shale. JOINTS to reservoir simulation workflow can represent hydraulic fracture geometry in a reservoir model while preserving fracture apertures. It can be very useful in investigating issues especially those pertaining to hydraulic fracture complexity and fracture aperture variations In the next two chapters; the workflow has been used to investigate two aspects of residual gel damage in hydraulic fractures and their effect on cumulative gas production. They are:

1) the effect of homogenous vs. heterogeneous gel damage in hydraulic fractures.
2) capillary pressure arising due to residual gel damage in hydraulic fractures, and

3.1 ASSIGNMENT OF CAPILLARY PRESSURE

Since no data was available for variation of capillary pressures with permeability in proppant packs, it was decided to use empirical relationships from the literature. Mattax et al. (1975) did core analysis of several samples of unconsolidated sands. Among other properties, they also studied drainage capillary pressures in these cores. The analysis was based on experiments performed on 20 cores. The permeability of these cores varied from 20 mD to 1.5 Darcy and porosity ranged from 15 % to 28%. The data was graphically correlated using the Leverett J-function as given in Figure 3.1.

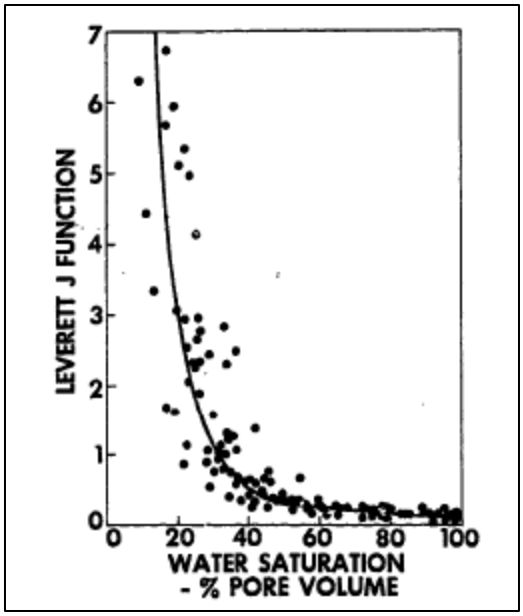

Figure 3.1: Leverett J-function plotted against water saturation for unconsolidated sands (from Mattax et al. 1975).

The values for Leverett J-function for each saturation are related to the permeability and capillary pressure as (Leverett et al. 1941).

$$P_c(S_w) = \frac{J(S_w).\gamma.\cos\theta}{\sqrt{\frac{k}{\phi}}} \tag{3.1}$$

or in field units

$$P_c(S_w) = \frac{461.6\,J(S_w).\gamma.\cos\theta}{\sqrt{\frac{k}{\phi}}} \tag{3.2}$$

where

$J(S_w)$ = value of Leverett J-function,

γ = surface tension for brine (dynes/cm),

k = permeability in mD,

φ = porosity, and

θ = contact angle in degrees.

Contact angle was assumed to be zero meaning the rock is water wet. The surface tension for brine was set to be 72 dynes/cm (Penny et al. 2012). Using the above equation, values of the Leverett J-function from Figure 3.1, and relative permeability curves, capillary pressure curves were determined at specific permeability and porosity. The relative permeability curves are the same ones used in Chapter 2 for the fracture to production workflow taken from Cheng et al. (2012) (Figure 3.2). Although specific values for capillary pressure at different water saturations were generated based on permeability of water calculated from absolute permeability and relative permeability curves, the relative permeability curves themselves were not modified with capillary pressures. In reality however, capillary pressure and relative permeability curves are affected by each other and any change in capillary pressure at a particular saturation would lead to a change in relative permeability of fluid (Christiansen 2001). This effect however has not been accounted for in our simulations. An example of permeability curve obtained for an absolute permeability of 100 mD is shown in Figure 3.4.

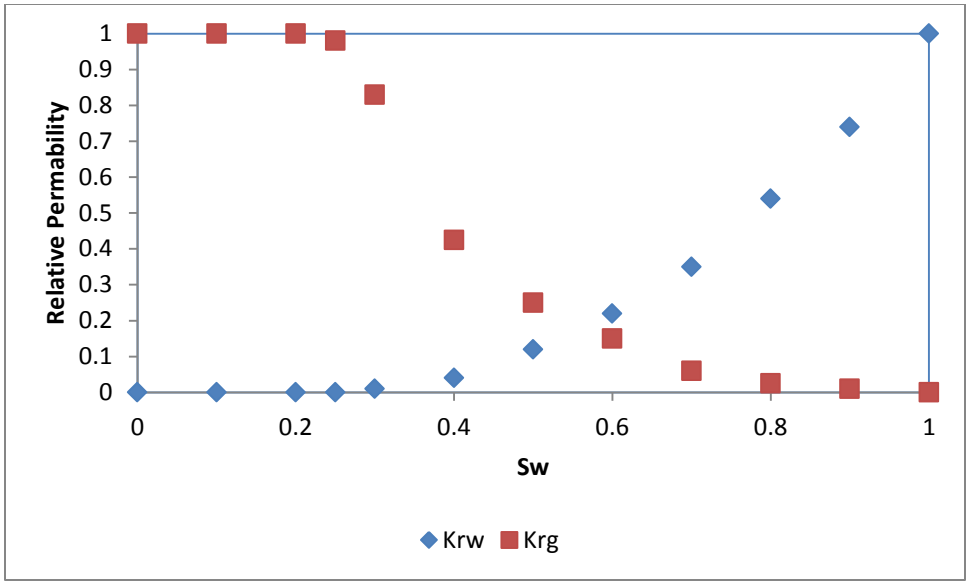

Figure 3.2: Relative Permeability curves for Matrix.

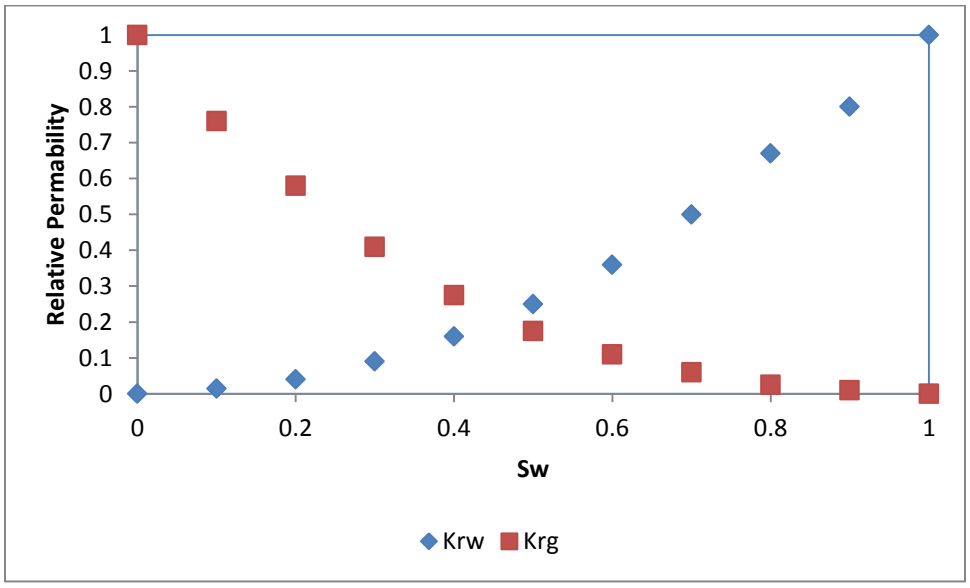

Figure 3.3: Relative permeability curves for fractures.

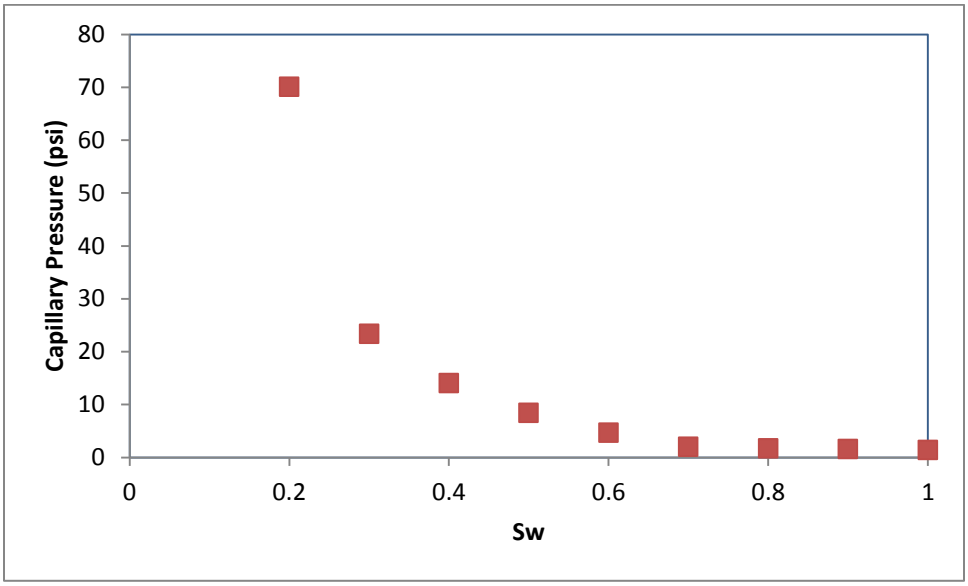

Figure 3.4: Capillary pressure curve for a fracture permeability of 100 mD.

3.2 SIMULATION SET UP

Fracture to production workflow provided in Chapter 2 was used to obtain a reservoir model containing hydraulic fractures. Fracture geometry and apertures were obtained from JOINTS modeling. The input parameters used for hydraulic fracture simulation were the same as in Table 2.5 except for grid size, thickness of the pay zone and number of fracture seeds. The dimensions of the grid block in x-y direction were doubled and the overall thickness of the formation was reduced to 45 ft. Thus each grid block was 13.12 ft. x 13.12 ft. in x-y dimensions. The number of fracture seeds representing natural fractures was increased to 700 to obtain a more complex hydraulic fracture network. As per the workflow, the output from JOINTS was then transferred to

the ECLIPSE reservoir simulator. The resulting hydraulic fracture network is provided in Figure 3.5 followed by basic parameters to be used for the reservoir model (Table 3.2).

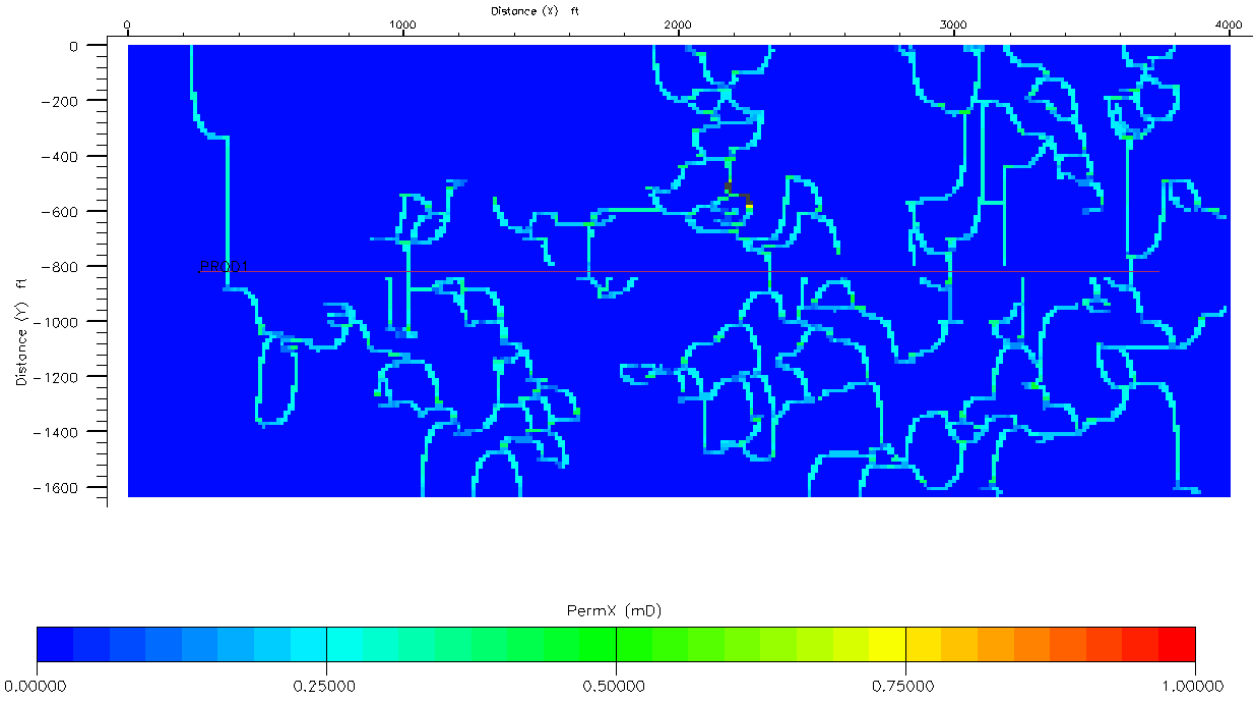

Figure 3.5: Permeability map of the reservoir model in ECLIPSE.

Reservoir Model Properties	
Reservoir Parameters	
Depth (ft.)	7000
Thickness (ft.)	45
Rock Properties	
Matrix Porosity	3.30%
Rock Compressibility (Psi^{-1})	$1x10^{-6}$
Fracture Porosity	40%
Proppant Permeability (mD)	1000
Well Parameters	
Wellbore Diameter (ft.)	0.325
Length of Lateral (ft.)	5200
Initial Condition	
Reservoir Pressure (psi)	3600
Water Saturation	0.15
Fluid Properties	
Standard Pressure (psi)	14.7
Standard Temperature (°F)	60
Reference Temperature (°F)	130
Grid Properties	
Number of cells in x-direction	305
Number of cells in y-direction	125
Number of cells in z-direction	3
Size of grid block (ft.)	13.12 x 13.12 x 15

Table 3.1: Basic reservoir model properties.

3.3 GEL DAMAGE DISTRIBUTION

It is understood that reduction in conductivity due to gel damage affects gas flow more adversely in parts of the fractures where conductivity is already low (Wang et al. 2009, Barree 2003). In the JOINTS to reservoir simulation workflow, discussed in Chapter 2, the permeability of the fracture network in the reservoir model is scaled according to fracture apertures provided by JOINTS thus fracture aperture information is incorporated into the reservoir model. Since fracture conductivity is a product of fracture permeability and width, lower width translates into lower fracture conductivity. This can be understood by considering the buildup of gel filter cake during gel damage on the fracture walls. The filter cake reduces available fracture width reducing fracture conductivities. Sections of hydraulic fractures which already have lower width will be effected even more adversely from this gel filter cake since the conductivity reduction will be much higher than in sections of hydraulic fracture networks which have higher widths. Hence, apertures can be used as criteria to determine whether a particular fracture cell in the reservoir model is damaged or not in a fracture network with heterogeneous damage. This is how heterogeneous fracture damage was introduced into our simulation cases, i.e. fracture grid cells with apertures below a threshold value were considered damaged and their permeability was adjusted to account for that. The damage was introduced during up scaling by reducing the permeability of the fracture grid cells in

EXCEL before importing them into the reservoir simulator. The average fracture width for our model was 0.04 inches and median fracture width was 0.043 inches (Figure 3.6). The permeability of the proppant without gel damage was assumed to be 1D, taking into account other damages such as proppant crushing, fines migration, and non-Darcy flow.

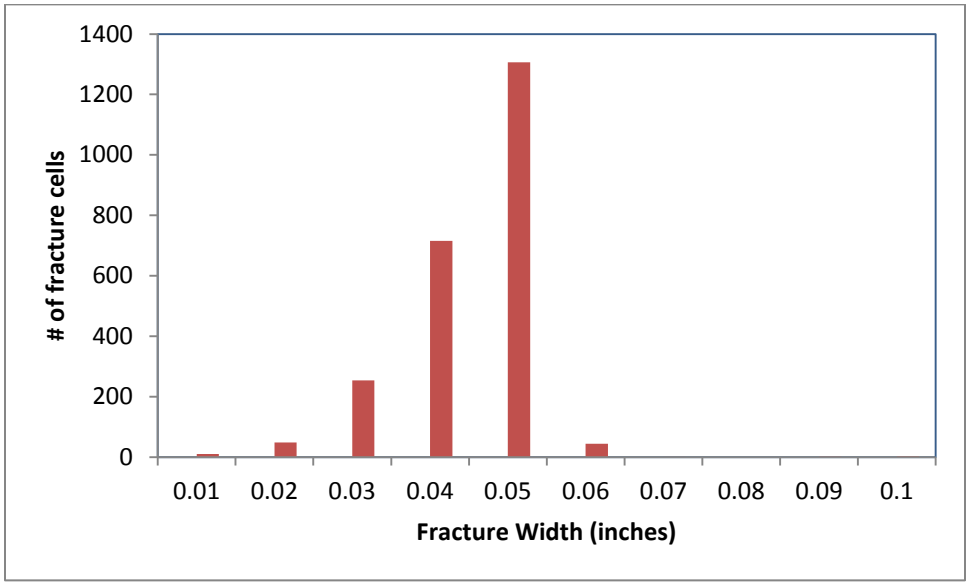

Figure 3.6: Fracture width distribution in the reservoir model.

3.4 Simulation Cases

Heterogeneous vs. Homogenous gel damage

Two values for permeability damage were assumed for a heterogeneously damaged case. First cases were run with a heterogeneous permeability damage of 100 mD (90% damage) whereas simulations were then run with a damage of 10mD (99% damage) for heterogeneous case. For each heterogeneous simulation case, an equivalent homogenous simulation case was also run with the fracture network assigned an average permeability value calculated from heterogeneous cases. This value is calculated using

equation 3.3. A number of simulation cases were run under each permeability damage with various values for the extent of gel damage with respect to the total length of the fracture network (Table 3.4).

$$k_{avg} = \frac{Dk_{damaged} + (100 - D)k_{Proppant}}{100} \tag{3.3}$$

Where

D = Percentage of hydraulic fracture network damaged in the heterogeneous case

$k_{Proppant}$ = original permeability of the proppant

$k_{damaged}$ = Permeability of proppant in damaged parts of the network for heterogeneous cases

k_{avg} = the permeability assigned to the fracture network to create an equivalent homogenous case.

Case #	Aperture Threshold (inches)	D (% of Damaged fracture grid cells in heterogeneous case)	K_{avg} (Equivalent average fracture Permeability for Homogeneous case)	
			d_{amaged} = 100 mD	d_{amaged} = 10 mD
i	0.035	26.80	758.7	734.6
ii	0.039	36.51	671.3	638.5
iii	0.043	48.36	564.8	521.3
iv	0.045	57.24	484.9	433.4
v	0.047	69.87	371.1	308.3
vi	0.048	76.43	312.2	243.4
vii	0.049	85.44	231.0	154.1
viii	0.059	94.44	150.1	65.1

Table 3.2: Simulation cases to study effects of heterogeneous vs. homogenous gel damage

Effects of capillary pressure with permeability variation in the damaged zone

To analyze the effects of introducing capillary pressure due to reduction in permeability in fracture network affected by gel damage, 4 scenarios were considered (Table 3.3). For each scenario, permeability in the damaged zone was varied from 99% to 10% (10mD to 900mD) of the original proppant permeability in a series of simulation runs. The range of permeability was chosen based on data available in the literature. The combined effect of residual gel damage and gel filter cake can itself cause a conductivity reduction of anywhere from 20% to as much as 1000$ the original conductivity and in extreme cases, eliminating conductivity altogether (Barree 2003). In lab experiments, effective conductivity of proppant was reduced to as little as 3% of the original value due to a number of physical phenomenon including but not limited to gel damage, multi-phase flow and non-Darcy flow. If the effects of proppant crushing and fines migration are added, it can go down to as low as 1% of the original proppant conductivity (Palisch et al. 2007). For each set, simulation runs were made considering capillary pressure in the damaged zone as calculated from Leverett function provided by Mattax et al. (1975). The simulations were then repeated with capillary pressure considered to be zero throughout the fracture network which is the common assumption while simulating production from hydraulic fractures both in industry and academia.

Scenario	Aperture threshold (inches)	Damaged fracture grid cells (%)
A	0.03936	36
B	0.04723	70
C	0.04841	80
D	Homogenous Damage	100

Table 3.3: Simulation cases to study effects of capillary pressure with permeability variation.

Effects of capillary pressure with pressure drawdown

Using scenario A from Table 3.3, with 36.5 % of the fracture network damaged and a damaged permeability of 100 mD (90% permeability damage), a series of simulation runs were made for pressure drawdowns ranging from 500 psi o 3000 psi. The cases were run in a similar manner as previously stated with each simulation run conducted with and without considering capillary pressure in the damaged zone. The results of these simulations and their significance has been discussed in chapter 4 in detail.

CHAPTER 4 INVESTIGATION OF RESIDUAL GEL DAMAGE: RESULTS AND DISCUSSION

This chapter pertains to the results and discussion of the simulation cases described in chapter 3. Significance of these results is also addressed later on. Cases are run for homogeneous and heterogeneous proppant permeability damage, with the magnitude of damage varying from 900mD to 100mD. In the heterogeneous cases, proppant permeability damage is correlated with fracture aperture. The role of capillary pressure changes caused by damage is investigated. Finally, pressure drawdown is examined as a way to remediate water blocking on gas production in damaged proppant packs.

4.1 IMPACT OF PROPPANT PERMEABILITY DAMAGE ON GAS FLOW

Using reservoir parameters provided in Chapter 3, we ran a series of simulation cases with 0%, 50%, 90% and 99% permeability damage in hydraulic fracture proppant packs, distributed homogeneously throughout the fracture network (Fig. 4.1). The gas rates start out low and gradually increase for all cases (Fig. 4.1c). This is because fractures which are saturated with water initially produce water. As more water is produced, the water saturation in the fractures decreases, the relative permeability of water goes down and that of gas increases leading to an increase in gas production rate. In cases with lower damage the gas production rate after achieving a peak, starts to decrease as the matrix beside the fractures is being depleted and the gas how has to flow

in from sections of the matrix that are further away from the fractures. In simulation cases with higher damage, the gas production rate stabilizes and does not decrease. This might be because the low permeability in the fracture prevents the rapid depletion of the sections of the matrix adjacent to the fractures conserving gas saturation in them therefore gas can still flow from these sections into the fractures over longer periods of time. Thus instead of decreasing, the gas flow rate stabilizes. The other observation is that the gas production rate decreases with increasing damage and hence the cumulative gas production also decreases as damage increases. Gas rate seems to be inversely proportional to water production rate. Once the water production rate approaches zero, the gas production rate approaches a constant value. From water production rates in Figure 4.1, it seems that the higher the damage, the less time it takes for the water production rate to go down to zero and hence for the gas production rate to attain a constant value. Thus with increased damage, water rates start out at lower values and approach zero much earlier leading to a lower cumulative water production. Initial water saturation in the fractures is the same for all cases; this also means that the percentage of recoverable water retained by fractures and the formation is increasing with increasing damage. It should be noted that all water produced is from the fracture since the water in the matrix is initially at residual water saturation.

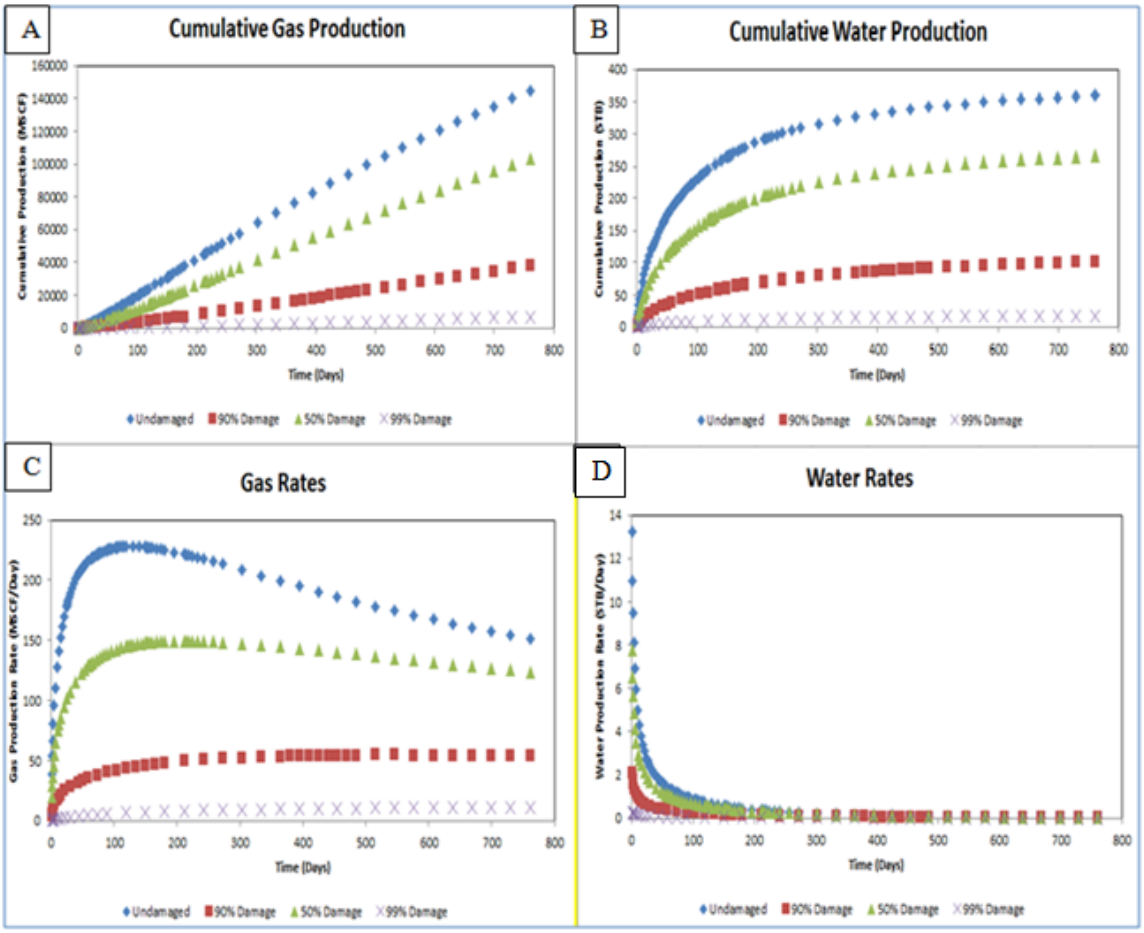

Figure 4.1: Cumulative production and rates over two years plotted for a range of permeability damage. A) Cumulative gas production B) Cumulative water production C) Gas production rate D) Water production rate

One other observation is that the rate of production of water goes nearly to zero within the first 200-300 days of production (Figure 4.2).This is also evident in the Figure 4.3, where the water cut goes down from around 1 to 1/1000 within the first 200-300 days but stays in the same order of magnitude for the remaining time. This means 2 years is an appropriate run time for our simulations since not much change in gas or water

production trends is expected after the first 300 days of production. This duration ensures that production trends and changes are adequately observed while saving computational time.

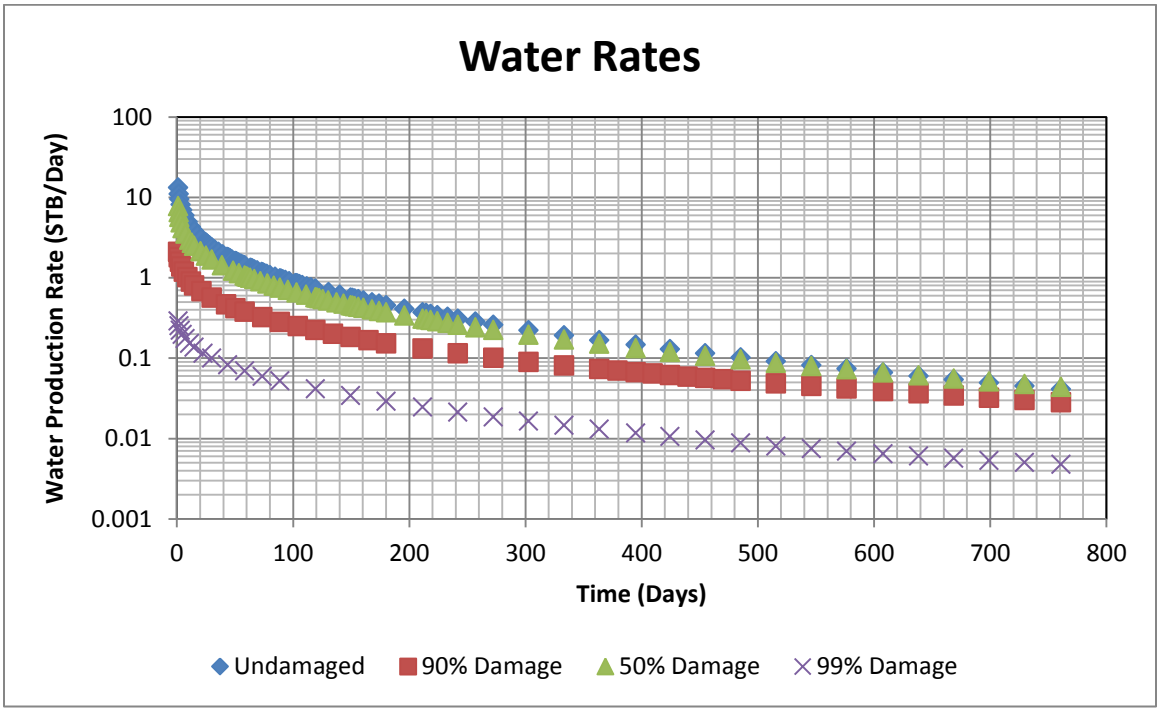

Figure 4.2: Water production rates for a range of damages over two years.

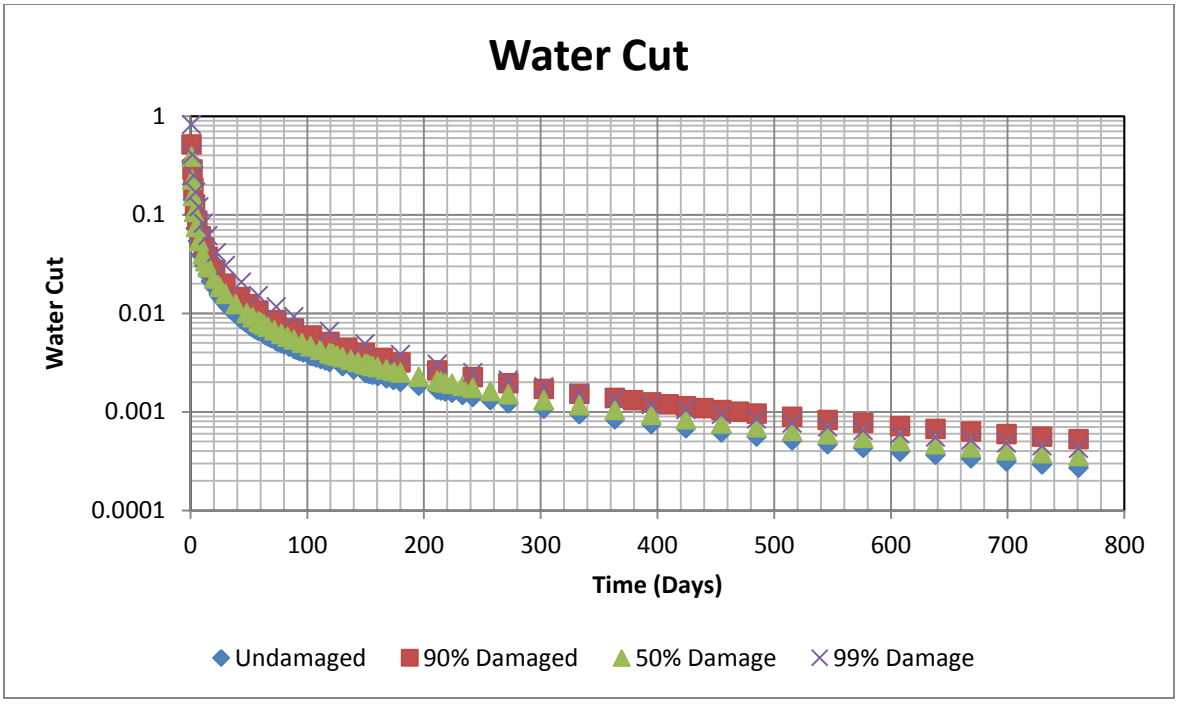

Figure 4.3: Water cut for a range of damages over two years.

4.2 HETEROGENEOUS VS. HOMOGENOUS GEL DAMAGE

As mentioned in Chapter 1, distribution of gel damage is hard to determine. Hence the damage is typically treated as homogenous. In order to evaluate whether considering heterogeneity in gel damage during reservoir simulations has an impact on production, several heterogeneous and equivalent homogenous cases were run. As mentioned earlier, damage is proportional to aperture for the heterogeneous case.

The permeability map given in Figure 4.4 for both homogenous and heterogonous cases demonstrates the differences in permeability distribution between a representative homogenous and heterogeneous case. In this particular case, 36% of the fracture network in the heterogeneous simulation case was 90% damaged with a permeability of 100 mD. This gives an equivalent average permeability of 671 mD for the homogenous case.

Certain branches in the fracture network, mostly the ones perpendicular to the general direction of propagation already have low conductivities due to lower apertures. The low aperture results from unfavorable stress distribution around these branches since they are opening up against S_{Hmax} (the maximum horizontal stress). With already low conductivities, when the proppant permeability in these branches is damaged by 90% in heterogeneous case, this reduces the conductivity even further and as a result many of these branches essentially become 'pinch points' where conductivity is so low that the flow through them is negligible. Thus parts of the fracture network that are connected to the main network through these branches become disconnected and cannot contribute to the gas production. For a homogenous case, the whole fracture network is equally damaged and the permeability throughout the fracture network is reduced to 671 mD which is the average permeability derived from the heterogeneous case. The same low aperture and thus low conductivity branches are present in this case. However,; the permeability reduction in this case is only 329 mD as opposed to 900 mD. Thus, the conductivity reduction is not as drastic as in the heterogeneous case, and the whole network still contributes, resulting in an overall higher cumulative production.

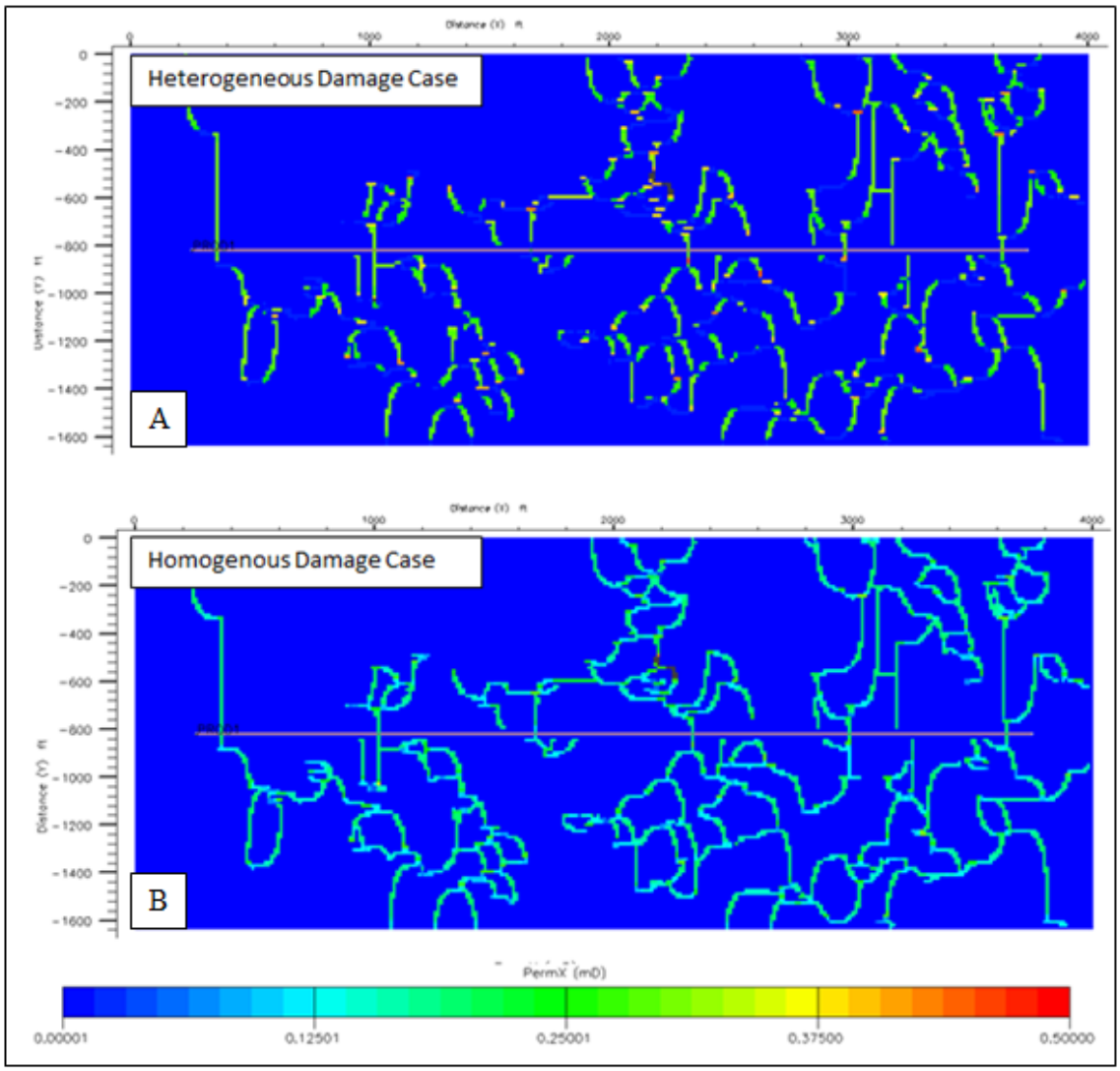

Figure 4.4: Permeability map depicting hydraulic fracture networks for both A) heterogeneous and B) homogenous damage cases when damaged heterogeneous permeability is 100 mD.

Figure 4.5 shows the results of simulation runs performed with a damaged permeability of 100 mD in heterogeneous cases. Cumulative gas production after 2 years is plotted vs. equivalent average permeability assigned to the fracture network in homogenous cases or k_{avg} which has been defined in the previous chapter. Reduction of

permeability and thus conductivity causes a reduction in cumulative production as observed in Figure 4.5. In our simulations for homogenous cases, the Fcd value ranges from 68.8 at fracture permeability of about 750mD to 13.8 at around 150 mD thus although these are high Fcd numbers, the fractures still have finite conductivity. Over this range, increasing the conductivity 5 times (from .55 mD-ft. to 2.75 mD-ft.), caused an increase in production from about 50000 MSCF to 125000 MSCF which is a reduction of about 2.5 times. Mayerhofer et al. (2006) changed their Fcd from 11.1 to 55.5 by changing the fracture conductivity from 2 mD-ft. to 10 mD-ft. and increased the cumulative production by twice in 2 years. Reese (2007) changed her Fcd from 13.3 to 66.6 by changing the fracture conductivity from 1 mD-ft. to 5 mD-ft. resulting in a production increase of 2.6 times over 2 years. Thus the change in production in our case for the same range of Fcd values is very much comparable to Mayerhofer et. al (2006) and Reese (2007). This comparison holds only for homogenous cases as there is no known example of the effect of conductivity on production for heterogeneous cases in literature.

It can also be observed that homogenous cases with same equivalent permeability gave a higher cumulative production then heterogeneous cases. As permeability map in Figure 4.4 shows, this is because of the parts of the hydraulic fracture network becoming disconnected from the main network due to extremely low permeability areas or pinch points formed due to higher reduction in permeability as compared to homogenously damaged cases resulting in them not contributing towards the overall production. It can also be observed that the rate of decrease in production with damage increases at higher

damage. There seems to be a threshold effect between average permeability of 300 and 200 mD after which the cumulative production dips. This may be due to a large section of the hydraulic fracture network becoming inaccessible due to a 'pinch point' forming after the percentage of damaged hydraulic fractures increases and average permeability changes from 300 mD to 200 mD (Figure 4.6). Once this section is disconnected from the rest of the network, it stops contributing in the production causing a rapid decline in production and it would remain disconnected unless the damaged is reversed.

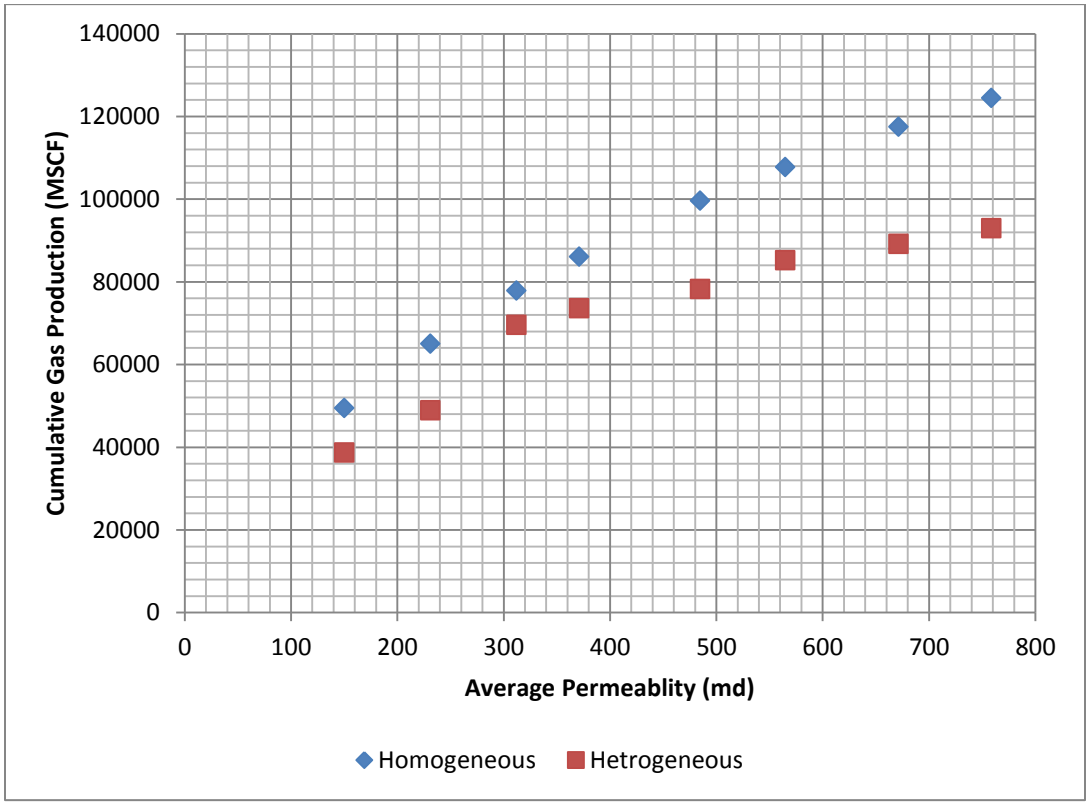

Figure 4.5: Cumulative gas production plotted against average permeability of the fracture network for both heterogeneous and homogenous gel damage cases.

The difference in how different sections of the hydraulic fracture network contribute towards production in homogenously and heterogeneously damaged cases can

also be seen from the pressure distribution around the wellbore (Figure 4.6). Almost all the network in the homogenous case is contributing to the production. However, in the case of heterogeneous damage, parts of the network that are disconnected remain at or close to reservoir pressure hence not producing any significant amount of gas. These parts are identified with arrows in Figure 4.6. If the permeability damage increases to 99% and thus the proppant permeability in the damaged zones decreases to 10mD, the differences in cumulative production between homogenous and heterogeneous cases become even more marked as shown in Figure 4.7.

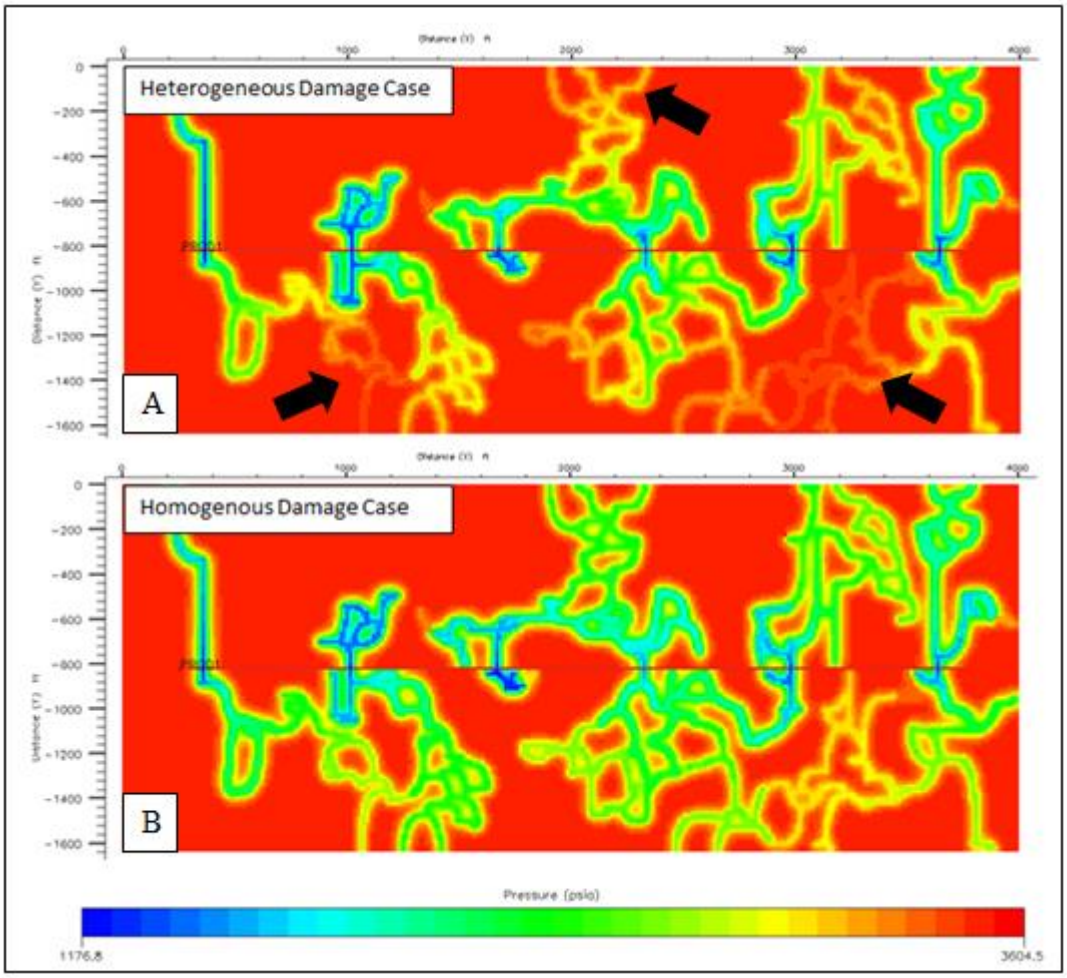

Figure 4.6: Pressure distribution after 2 years of production around the well for both A) heterogeneous and B) homogenous damage cases when damaged heterogeneous permeability is 100 mD

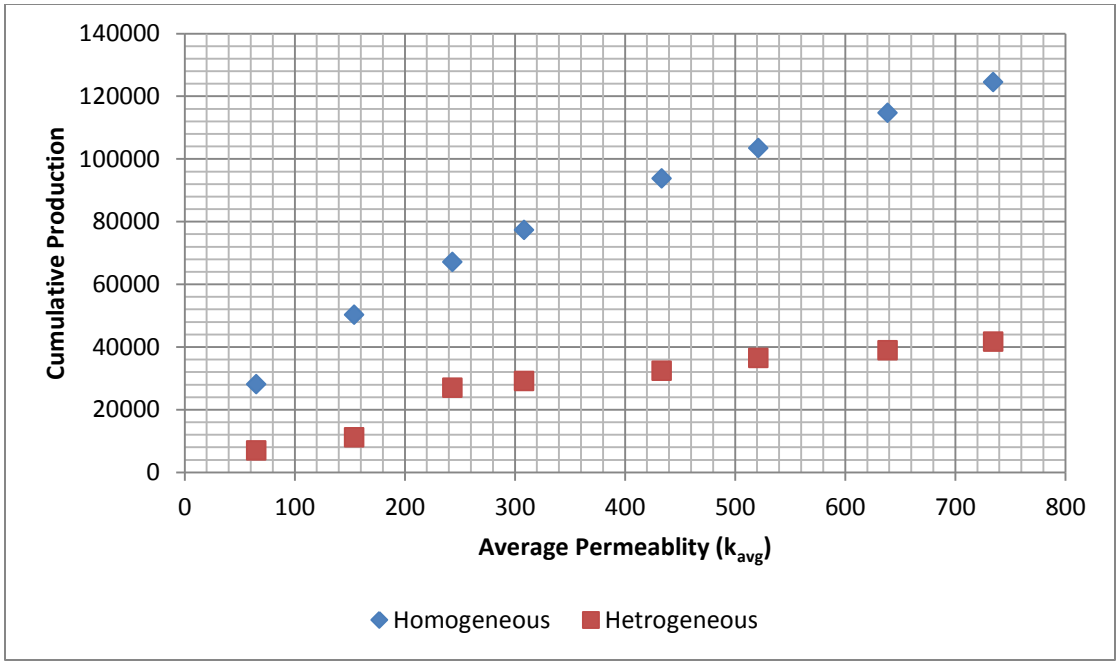

Figure 4.7: Cumulative gas production plotted against average permeability of the fracture network for both heterogeneous and homogenous gel damage when heterogeneous damaged permeability is 10 mD.

Again, the underlying cause for the difference in production is the occurrence of pinch points due to decrease in permeability, only this time, since the permeability reduction is higher for heterogeneous case, there are many more 'pinch points' hence a larger portion of the fracture network is disconnected and unable to contribute in production. This is clear from the permeability map given in Figure 4.8. This effect is even more evident in the pressure distribution around the well bore (Figure 4.9) for the heterogeneous case where most of the production takes place within the immediate vicinity of the well bore and most of the network further away from the well bore is essentially cut off from the well bore and does not contribute to production.

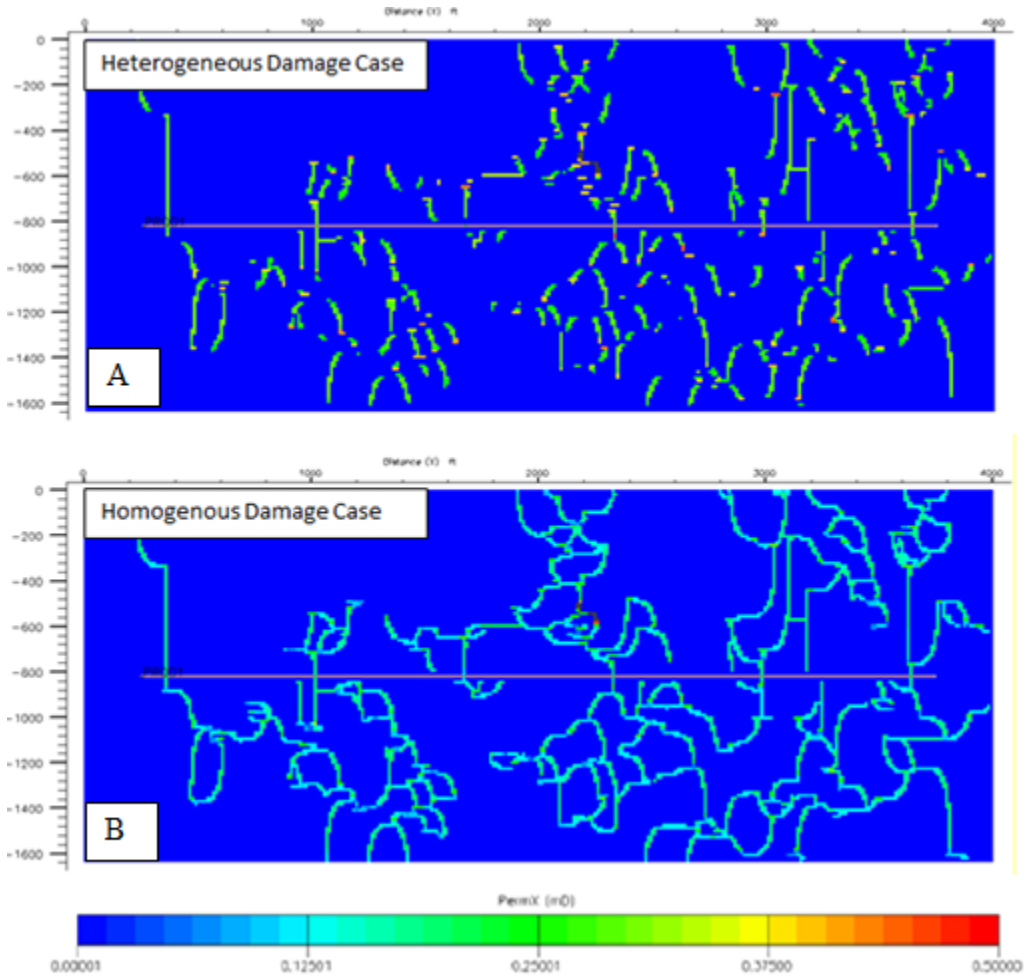

Figure 4.8: Permeability map depicting hydraulic fracture networks for both A) heterogeneous and B) homogenous damage cases when damaged heterogeneous permeability is 10 mD.

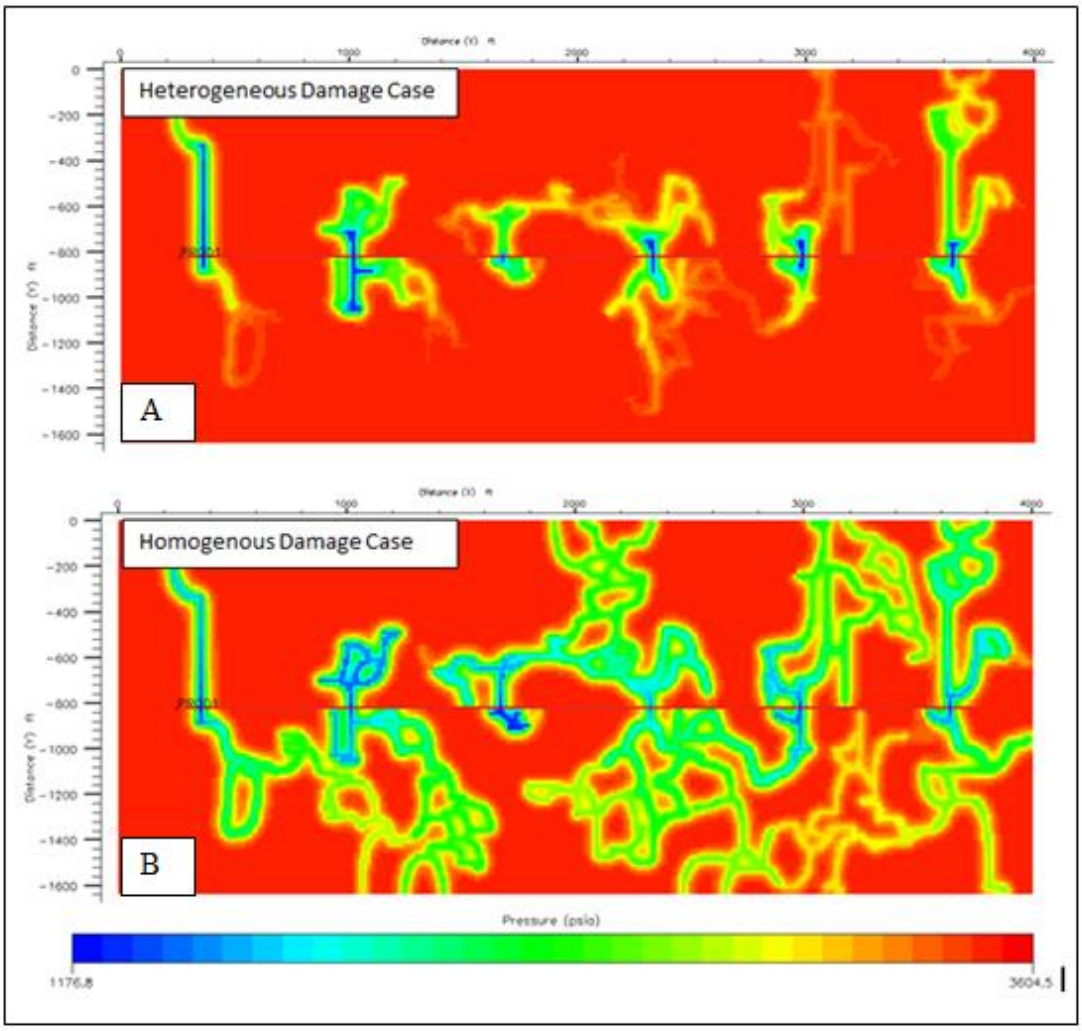

Figure 4.9: Pressure distribution after 2 years of production around the well for both A) heterogeneous and B) homogenous damage cases when damaged heterogeneous permeability is 100 mD.

The differences in production between homogenous and heterogeneous case are quite large. In Figure 4.10, the difference in cumulative gas production between homogenous and heterogeneous cases for each average permeability is plotted as a

percentage of cumulative production in homogenous case. When damage is 90%, the difference between cumulative productions is about 10-20% which is significant. However, with 99% damage and further permeability reduction, the difference goes into the range of 60-80% which is very high and would cause severe inaccuracies in production forecast.

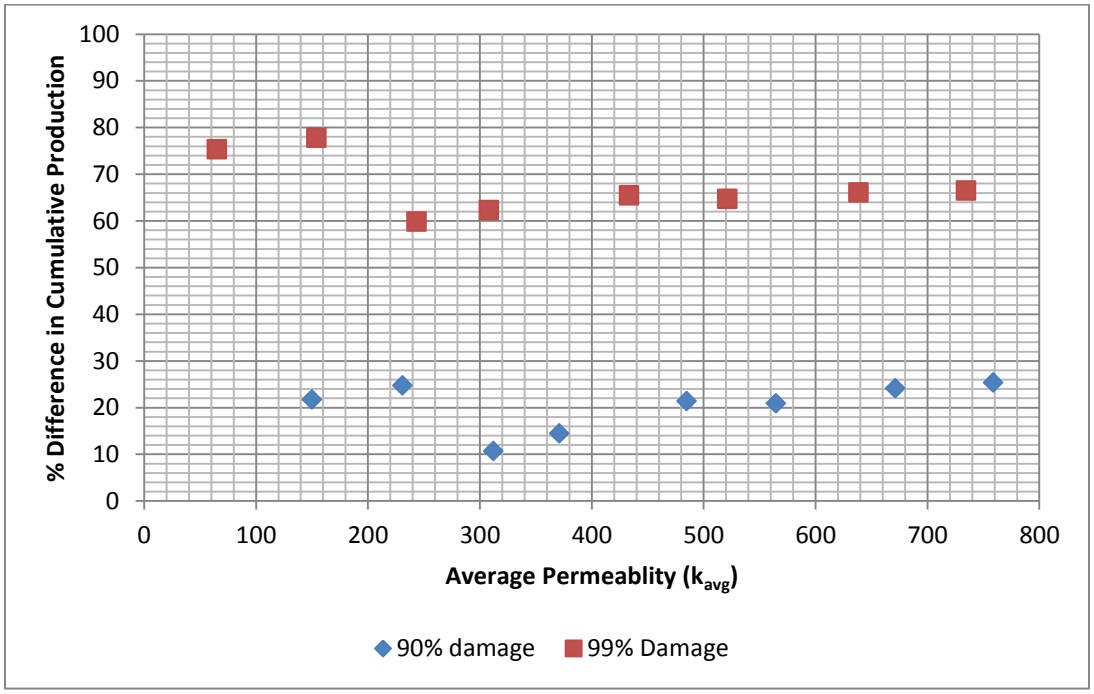

Figure 4.10: Percentage difference in cumulative production between heterogeneous and homogenous gel damage cases plotted against average permeability of the fracture network.

4.3 EFFECTS OF CAPILLARY PRESSURE WITH PERMEABILITY VARIATION IN THE DAMAGED ZONE

Capillary pressure is routinely assumed to be zero in hydraulic fractures during reservoir simulation however, in cases where there is permeability reduction due proppant gel damage, capillary forces might be present. Simulations were run to study the effect of capillary pressure on gas production using cases described in Chapter 3. The heterogeneous cases were run with varying degrees of network damage, and these are compared to each other and a homogeneous damage case. The three heterogeneous cases had 36%, 70% and 80% of their fracture network damaged based on fracture aperture as described in Chapter 3.

Figure 4.11 and 4.12 represents the results of the simulations performed to study the effect of capillary pressure on cumulative production over a range of permeability damage. In each case, a simulation is run with capillary pressure in the damaged zone and is then repeated while assuming the capillary pressure in the damaged zone to be negligible. The difference in cumulative production between both runs is plotted against permeability damage,

$$\Delta G_{Pc} = (G_{Pc=0} - G_{Pc\neq0})\ 100 / G_{Pc=0} \qquad (4.1)$$

Where

ΔG_{Pc} = % Difference in Cumulative Gas Production

$G_{Pc=0}$ = Cumulative gas production for cases where capillary pressure in damaged zones is considered zero

$G_{Pc\neq0}$ = Cumulative gas production for cases where capillary pressure in damaged zones is not zero.

Similarly, for water;

$$\Delta W_{Pc} = (W_{Pc=0} - W_{Pc\neq 0})\ 100 / W_{Pc=0} \qquad (4.2)$$

Where

ΔW_{Pc} = *% Difference in Cumulative Water Production*

$W_{Pc=0}$ = Cumulative water production for cases where capillary pressure in damaged zones is considered zero

$W_{Pc\neq 0}$ = Cumulative water production for cases where capillary pressure in damaged zones is not zero.

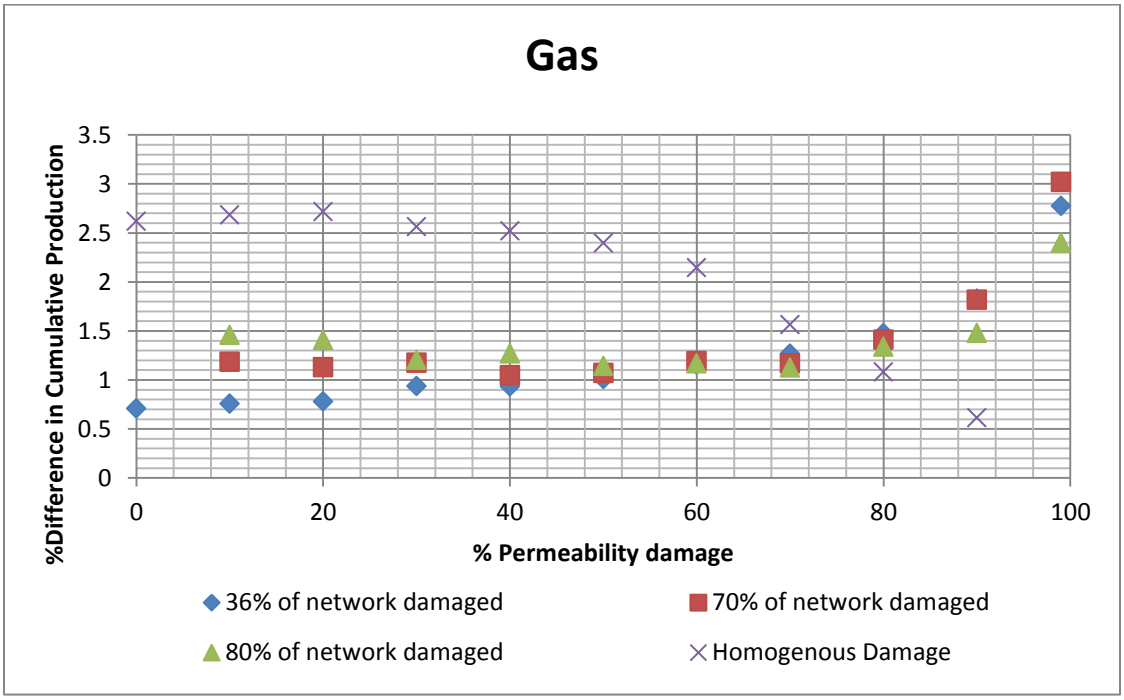

Figure 4.11: Percentage difference in cumulative gas production between cases with P_c=0 and $P_c\neq$0 after 2 years plotted against percentage permeability damage. The three curves represent different extent of damages to the overall fracture network.

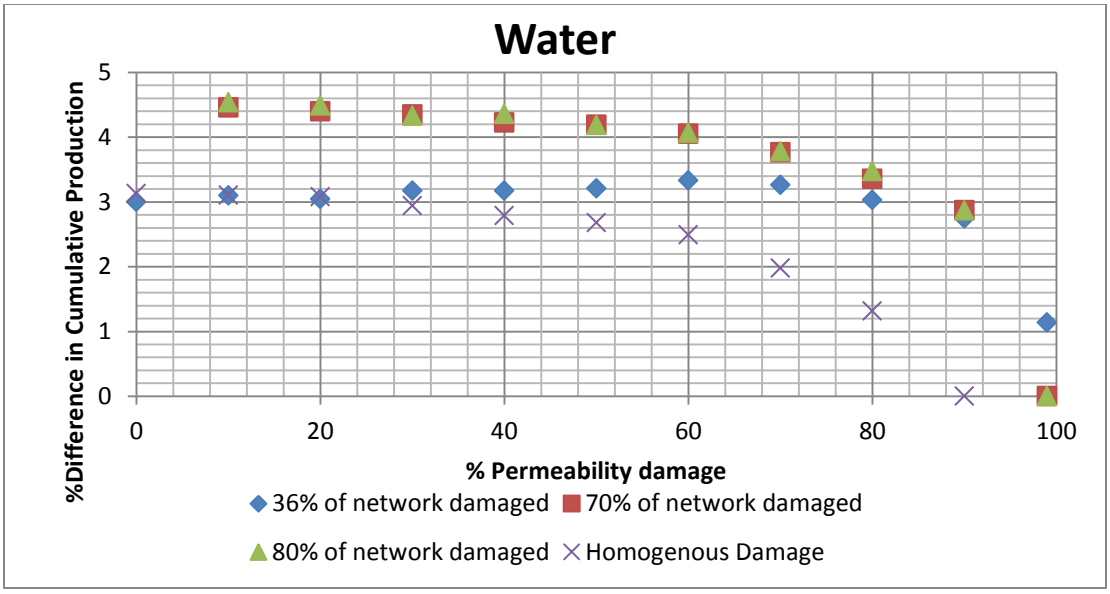

Figure 4.12: Percentage difference in cumulative water production between cases with Pc=0 and Pc≠0 after 2 years plotted against percentage permeability damage.

The first observation that can be made in Figure 4.11 is that all values are positive i.e. $G_{Pc=0} > G_{Pc\neq0}$ and this was observed in all the cases that were run in this study. Capillary pressure in the damaged zones of the fracture network makes it harder for the gas to move into those damaged zones and displace the fracturing fluid. As a result these parts of the fracture network maintain a high water saturation which hurts the relative permeability to gas. Cumulative water production is also higher in cases without capillary pressure compared to the cases with capillary pressure i.e. $W_{Pc=0} > W_{Pc\neq}$. If we consider the homogenous case, we observe that the difference in cumulative gas production between cases with and without capillary pressure is decreasing with increasing permeability damage. Water production for both homogenous and heterogeneously damaged cases seems to be following the same trend where the percentage difference in

water production is decreasing with increasing permeability damage (Figure 4.12). For heterogeneous cases, it can be observed that the difference in gas production between cases with capillary pressure in damaged zones and cases where capillary pressure is zero is high when the permeability damage is high but decreases for lower damage and becomes more or less constant after 70% permeability damage and does not change significantly after that. This trend is opposite to the trend seen in homogenous cases, even though the trend for water production is the same for both homogenous and heterogeneous cases.

These trends can be explained by considering the water saturation maps of the simulation cases. Figure 4.13 provides the water saturation distribution after 2 years for identical cases run with and without considering capillary pressure in the damaged zones. It can be seen that even after 2 years, when the capillary pressure in the damaged zones is non-zero, certain branches of the fracture network still retain water (identified by arrows in Figure 4.13). As a result, these branches are not able to contribute as much to gas production since the relative permeability for gas remains low, leading to a lower cumulative gas production.

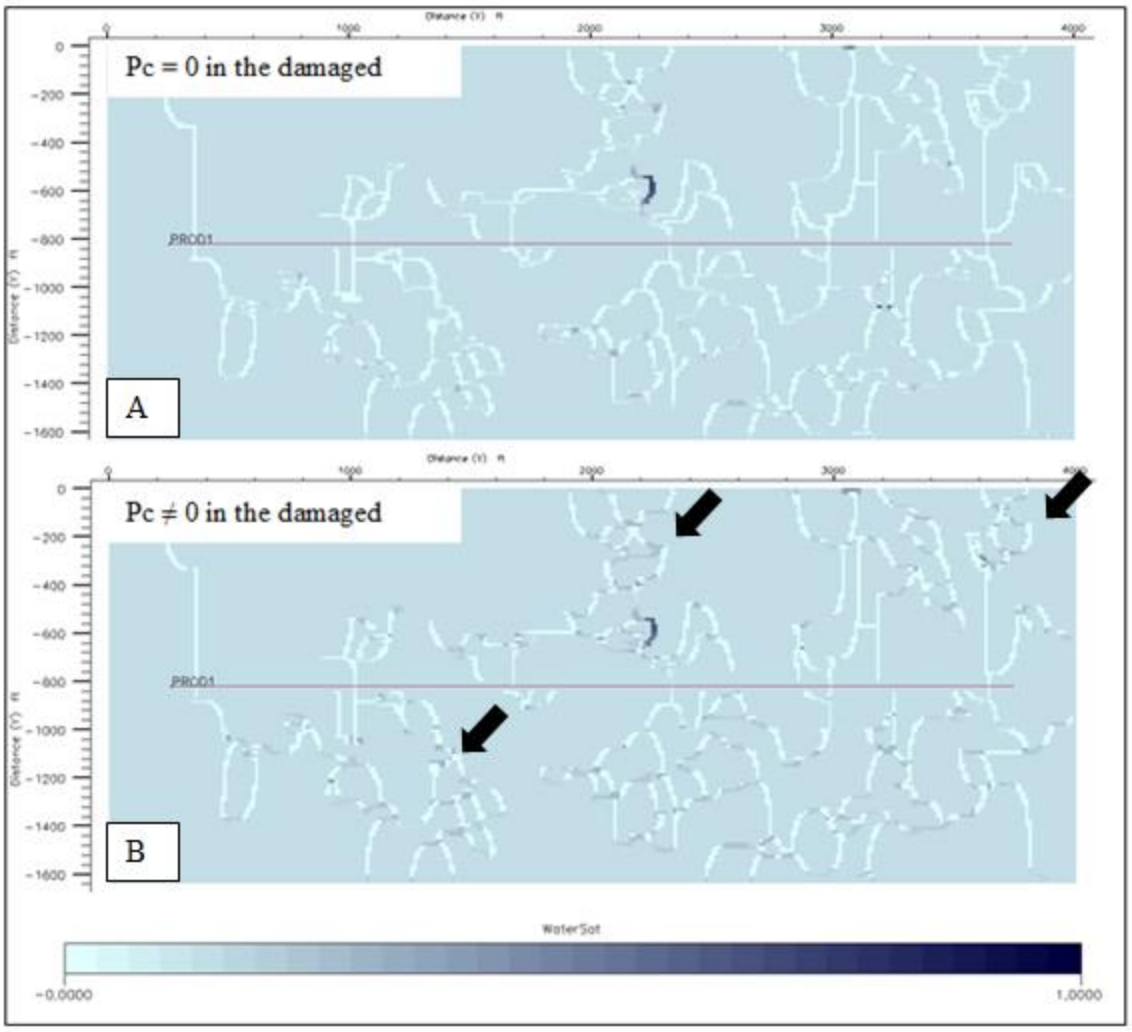

Figure 4.13: Saturation map of the reservoir grid after 2 years of production for A) Pc=0 and B) Pc≠0

It was observed in Figure 4.1 that the percentage difference between cases with and without capillary pressure in homogenously damaged cases was increasing with increasing permeability damage. This can be understood by considering Figure 4.14 which provides the saturation maps for homogenously damaged simulations cases run

with 90% and 50% permeability damage, with and without capillary pressure. One important observation that can be made in Figure 4.14 is that the difference in water retained in fractures between cases with and without capillary pressure seems to be higher in the 50% case. Even more interestingly, it can be seen that the higher difference is due to the fractures in the case for Pc=0 getting flushed more effectively when damage is 50%. The water saturation in that case in the fracture is almost zero. In the case when damage is 90% and Pc=0, there is still water saturation in the fractures. Thus it seems that alongside capillary pressure, permeability also plays a major role in water retention for homogenously damaged cases. Capillary pressure in the fractures helps in water retention over the entire range of damaged permeability. However, when there is no capillary pressure, the water retention is entirely a function of the permeability of the proppant and time but as seen in Figure 4.2, over the entire range of simulation parameters that we used, water production rate goes almost to zero within the first year of production. Hence, the difference in production with and without capillary pressure over the entire range of permeability damage for two years of production is essentially a function of capillary pressure and permeability. With decreasing damage, permeability increases, and capillary pressure (dependent on permeability) decreases thus the capillary pressure trend is favoring higher water and thus gas production. Permeability trend is also favoring higher water and gas production, however, as seen from Figure 4.14, decrease in capillary pressure from 90% damage case to 50% damage case is still not causing a drastic difference in water retention and fractures still seem to be saturated with water when Pc≠0 for the 50% damage case. Permeability increase from 90% damage case to 50%

damage case however, seems to cause the fractures to lose almost all water as visible in cases when Pc=0. Thus throughout the entire range of homogeneous damage simulation cases run, permeability change has a much higher effect than capillary pressure change. As damage decreases, the rise in production due to permeability increase of the fracture is much higher than the rise due to decrease in capillary pressure, thus the overall difference in production between cases with and without capillary pressure increases with decreasing permeability damage. In terms of equation 4.1, when permeability damage is decreasing $G_p \neq 0$ is increasing due to decrease in capillary pressure whereas $G_p = 0$ is increasing due to permeability increase. $G_p = 0$ is increasing at a higher rate than $G_p \neq 0$ thus the difference between the two is increasing with decreasing permeability damage.

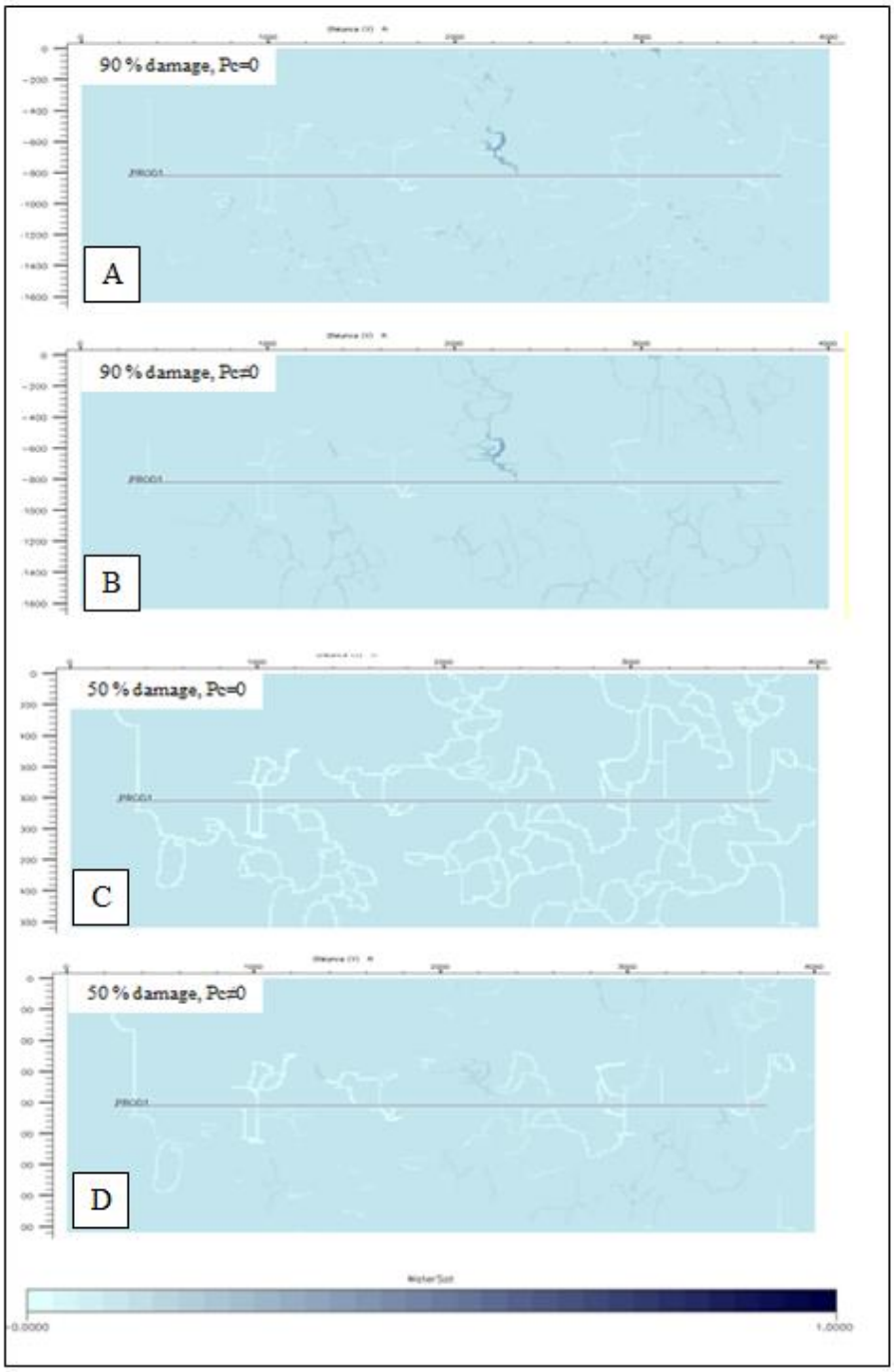

Figure 4.14: Water saturation maps for homogenous permeability damage cases after 2 years of production. A) 90% damage, Pc=0 B) 90% damage, Pc≠0 C) 50% damage, Pc=0 D) 50% damage, Pc≠0

For heterogeneous cases it was observed in Figure 4.12 that that the percentage difference between cases with and without capillary pressure in was decreasing with increasing permeability damage. To analyze this trend, we consider a representative case where 70% of the fracture network has 99% damage. In this instance, the difference in percentage water production between cases with and without capillary pressure is zero hence the water production profile are the same for both the cases. However, the difference in gas production is about 3%. It can be seen that if we consider gas flow rates for this simulation, the rates are more or less the same for the first 6 months or so but after that, the gas production rate for the case without capillary pressure is higher (Figure 4.15). This seems to indicate that the difference in production profiles between the two cases takes place when parts of the fracture network that are further away from the well bore start contributing towards production. Most of the damage is also in these distant sections since they are the ones with lower apertures.

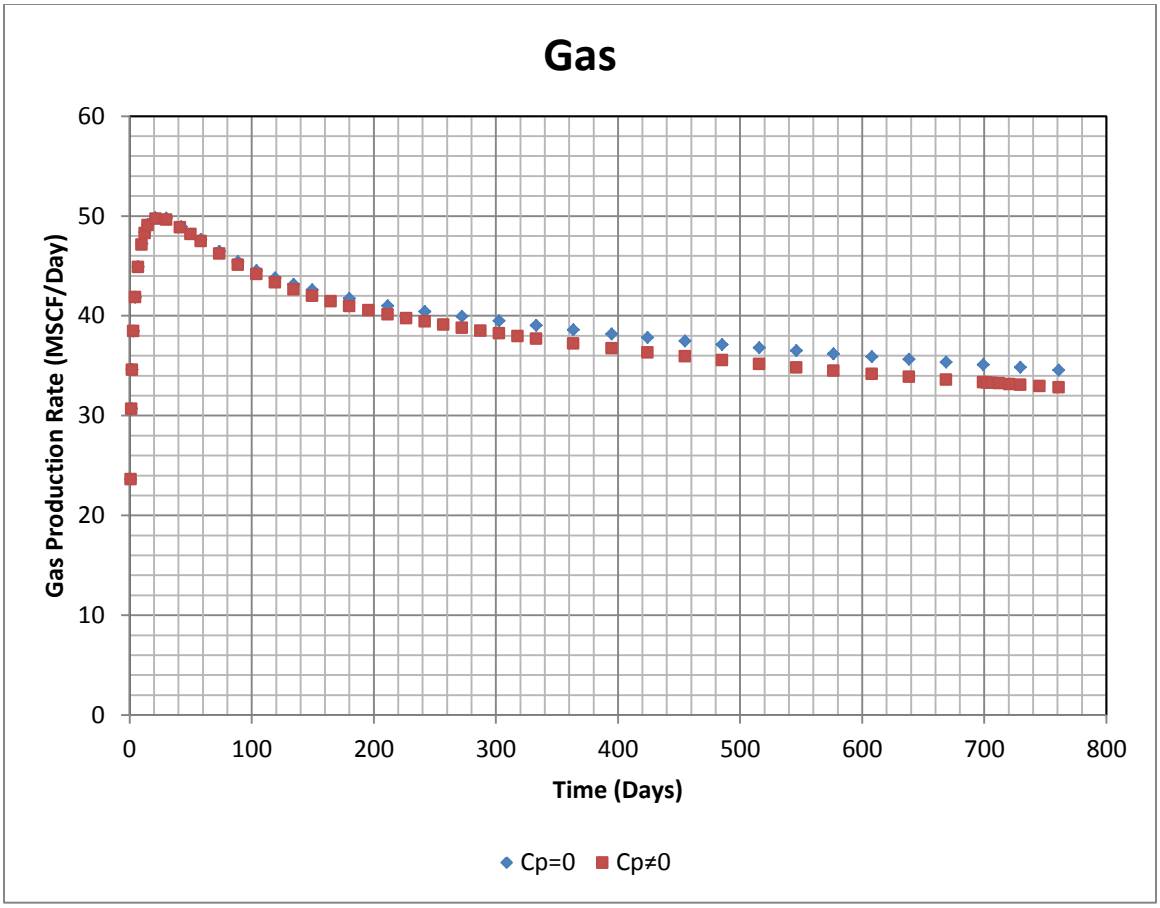

Figure 4.15: Gas production rates for the heterogeneously damaged case with 90% permeability damage and 70% of the fracture network damaged.

Water production profiles for both cases are the same thus at the time when difference arises between the two gas production profiles, the fractures for both cases are at same water saturation and relative permeability is also the same. However, in the simulation case where $P_c=0$, it is easier for the gas to flow into the fracture from the matrix since there are no capillary forces present in the fracture. In case where $P_c\neq0$, at the same water saturation, there is capillary pressure and hence capillary forces opposing the entry of gas into the fracture. Therefore, the gas saturation in fractures is lower

especially in the damaged zones and hence the overall gas production rate is also lower. This effect increases with increasing permeability damage as it can be seen in the Leverette J function provided in Equation 3.1 in which permeability has inverse square relationship with capillary pressure. Lower permeability means higher capillary pressure and thus higher difference in percentage difference in cumulative production between cases with and without capillary pressure. The reason this effect is not seen in homogenous cases is because the permeability damage occurs over the entire network and has a more dominating effect on production then it would have in heterogeneously damaged cases therefore decrease in production caused by permeability reduction due to damage masks the effect of increasing capillary pressure in homogenous cases.

4.4 Effects of Capillary Pressure with Pressure Drawdown

Holditch (1979) studied the effects of water blocking on gas production using a two phase, 2D finite difference model. When a well is fractured, some of the fracturing fluid leaks into the reservoir adjacent to the fracture which is thus referred to as the invaded zone. This increases the water saturation in this invaded zone as well as the capillary pressure and reduces the relative permeability to gas. Holditch also determined that the reduction of gas production as a result of water blocking is influenced by pressure drawdown. Higher drawdown can overcome the effect of the high capillary pressure in the damaged zone and thus the effect on gas production is minimal. With lower draw down, the capillary effects of the invaded zone cannot be overcome and thus the adverse effects on gas production are also increased. Holditch's results are given in

Figure 4.7. The graph on the left is cumulative production from a reservoir with invasion zone having higher capillary pressure with 325 psi drawdown where as the one on the right is with 1325 psi drawdown.

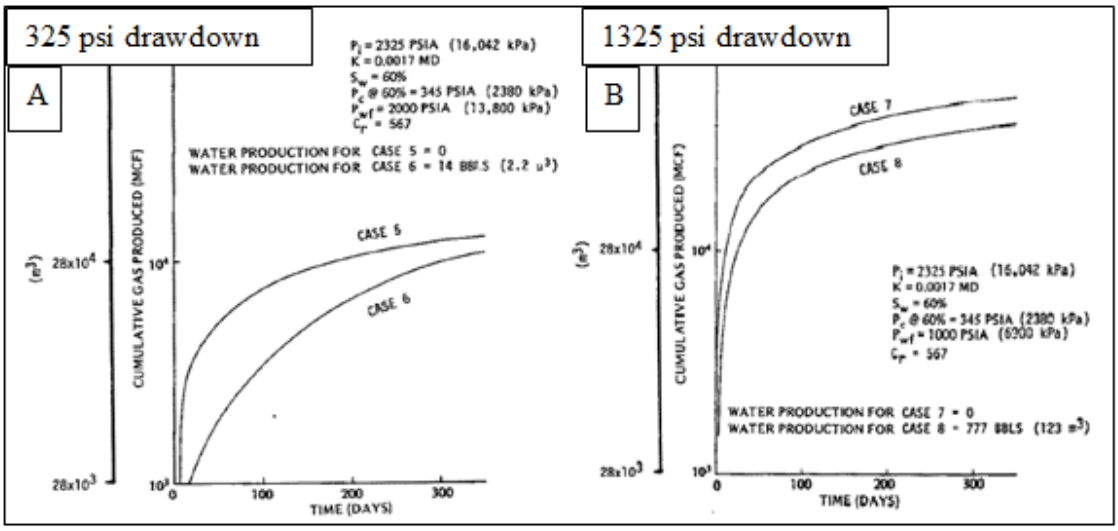

Figure 4.16: Difference in cumulative gas production between A) low and B) high pressure drawdown with a 345 psi Capillary pressure acting in the invasion zone. (from Holditch 1979).

When analyzing reduction in permeability in a fracture network and the introduction of non-zero capillary pressures as a result of that, the situation is quite similar to an invaded zone in the matrix adjacent to the hydraulic fractures discussed by Holditch. The obvious difference is that the damaged zone in our case occurs inside the fracture network and not in the matrix and thus the capillary pressure does not go as high as it would in an invaded zone in the matrix. However, the principle that drawdown can overcome capillary pressure blockage is the same hence we expect similar results when we evaluate the effects of pressure drawdown on cumulative production.

Figure 4.17 represents the results of the simulations performed to study the effect of pressure drawdown on capillary effects inside the hydraulic fracture network. The simulation case used had 36.5% of the fracture network damaged with a damaged permeability of 100mD (90% damage). In each case, a simulation is run with capillary pressure in the damaged zone and is then repeated while assuming the capillary pressure in the damaged zone to be zero. The percentage difference in cumulative production between both runs is plotted against pressure drawdown in the same way as it was previously plotted against percentage permeability decrease in the previous section. It can be seen that the difference in cumulative production between simulation runs with and without considering capillary pressures decreases with increasing pressure drawdown i.e. the effect of capillary pressure decreases with increasing drawdown. As mentioned previously, capillary pressure in the damaged zones of the fracture network makes it harder for the gas to move into those damaged zones and displace the fracturing fluid. The driving force for the influx of gas into the fracture network is the pressure drawdown. Higher drawdown makes it easier for the gas to overcome the capillary forces and flow from the matrix into the damaged zones of the fracture network, ultimately flowing to the surface, leading to a higher cumulative production. The opposite is true for lower pressure drawdown hence it can be seen that the reduction in cumulative gas production is high at lower drawdowns but gradually this difference decreases as drawdown increases.

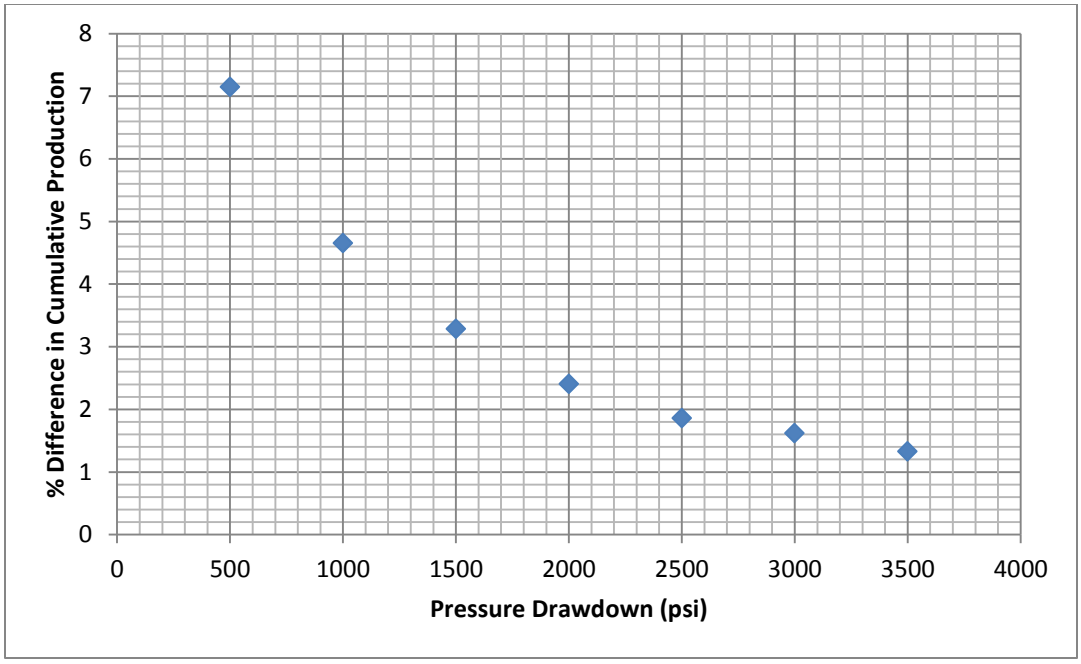

Figure 4.17: Percentage difference in cumulative gas production between cases with $P_c=0$ and $P_c\neq0$ after 2 years plotted against pressure drawdown.

It should also be noted that drawdown which for Figure 4.17 has been defined as the difference between bottom hole flowing pressure and reservoir pressure is not the same throughout the fracture network. Pressure distribution in the hydraulic fracture networks varies depending upon the conductivity of the fracture and its distance from the wellbore therefore different parts of the fracture network would have different drawdowns. Hence the ability to overcome the capillary forces would also vary where parts of the network nearer to the wellbore would have a higher drawdown and hence would be able to overcome the effects of capillary pressure more easily then sections that are further away.

4.5 SIGNIFICANCE

Gel damage can cause conductivity reduction anywhere from 20% to completely plugging up pores in the proppant pack and hence removing all conductivity. This reduction in conductivity can lead to significant loss of production as evident from literature and our simulation results. Conductivity loss of 80% which according to the literature can easily happen in hydraulic fractures, caused cumulative production over two years to be reduced by 2.5 times. Studies performed by Mayerhofer et al. (2006) and Reese (2007) give similar values for change in production due to change in conductivity.

When the effect of assuming homogenous damage vs. heterogeneous damage was studied, it turned out to have a very significant impact on cumulative gas production. When the permeability is 90% damaged in heterogeneous cases, the percentage difference in cumulative production when plotted against equivalent homogenous permeability ranges between 10-20%. Not accounting for the heterogeneity of the proppant damage consequently could results in significant overestimates of the cumulative gas production. This is a significant difference. However, when the permeability damage goes to 99% i.e. fracture permeability of 10 mD, the percentage difference rises to 60-80% which is extremely high and means that if heterogeneity is not accounted for, the cumulative production forecast will overestimated by about two-thirds of the actual value. As mentioned before, literature suggests that permeability reduction of 99% due to proppant damage is very much possible, thus assuming homogenous damage equally over the whole network in a reservoir simulation instead of the more

likely heterogeneous damage will lead to an over estimation of production especially in cases where gel damage is severe.

The effect of capillary pressure variation on cumulative production for three years over a range of damaged permeability in the hydraulic fractures was analyzed for homogenous and three heterogeneous cases. For both homogenous and heterogeneous cases, the percentage difference in cumulative gas production over the entire range of permeability damage which is 90% to 10% in this scenario did not exceed 3%. It should be noted that the bottom-hole pressure in all these cases was 1000 psi. Hence, in practical terms, ignoring capillary pressure in damaged parts of the hydraulic fracture network does not really impact the accuracy of production forecasting from reservoir simulations to a large extent at least at the Bottom-hole pressure of 1000 psi.

Later, the effect of pressure drawdown was investigated using a case from the previous scenario. The extent of damage was 36% with permeability damage of 90% (100 mD). The percentage difference in cumulative production ranged from about 1% at 3500 psi to 7% at 500 psi drawdown. The drawdowns at which wells are normally operated in shale formations are 2000 psi or larger. At these drawdowns, ignoring capillary pressure in reservoir simulations might not make a huge difference in production forecasting. However, in extreme cases where completion or geological constraints limit the bottom-hole pressure, ignoring capillary pressure might cause significant inaccuracy in predicting reservoir performance.

CHAPTER 5

CONCLUSIONS AND SUGGESTIONS

In this study, a fracture to production workflow was developed using the JOINTS, multi-fracture crack propagation software and ECLIPSE, a commercial reservoir simulator. The workflow was validated using a real data set from literature. Later, the workflow was used to investigate different phenomena pertaining to residual gel damage in hydraulic fracture networks. First was the presence of heterogeneous rather than homogenous damage in the hydraulic fractures. Second was the rise of capillary pressure due to permeability reduction in the damaged hydraulic fractures. In this section, we summarize the work and conclusions of our study. We also present some improvements and further work that can be undertaken to enhance and improve on what has already been done in this project.

5.1 SUMMARY AND CONCLUSIONS

Hydraulic Fracture to Production workflow

- A simple reservoir model was set up and validated against analytical solutions by Wattenburger et al. (1998) and type curves by Agarwal et al. (1979). It was shown that using large grid blocks for representing hydraulic fractures in reservoir models will not lead to any inaccuracies provided that fracture conductivities are scaled accordingly. Our simulation results matched very well with Wattenburger's analytical solutions and for late time with Agarwal's type curves.

- Natural fracture distribution characteristics such as fracture spacing and orientation has a large influence on hydraulic fracture geometry. There are two dominant fracture sets in Marcellus, J1 and J2 was determined from literature. Spacing for the J1 set, was through JOINTS modeling based on geo-mechanical properties determined from rock samples in the lab. For the spatial distribution of J2, outcrop data was used.
- A JOINTS model was also used to create hydraulic fracture network in the presence of the natural fractures. The SRV for this simulation was conditioned to available micro-seismic data. Hydraulic fracture properties including fracture geometry and apertures were then up scaled and transferred to ECLIPSE. A history match was conducted using production data available in the data set.
- The reservoir properties used to achieve a history match were similar to that used by Ajayi et al. (2011) hence validating the workflow and proving that it can be used for production forecasting and optimization with the same accuracy as other methods currently being used in the industry.

Heterogeneous vs. Homogenous gel damage

Simulations were run with both heterogeneous and equivalent homogenous proppant permeability damage. The mechanism postulated for permeability damage was gel residue. Heterogeneity in damage was based on fracture apertures. The damaged portions for the heterogeneous damage cases had proppant permablities of 100 mD (90% damage) and 10 mD (99% damage).

- Changes in production caused by alteration of conductivities in our simulation cases were found to be similar to those found in literature.
- Cumulative gas production over two years dropped by about 73% with 90% proppant permeability damage compared to a case with no damage.
- It was found that cumulative gas production for heterogeneous damage cases was always lower then homogenous cases with the same average fracture permeability. This is because some parts of the fracture network in heterogeneously damaged fracture network undergo a large reduction in permeability, essentially becoming pinch points and isolating other parts of hydraulic fracture network. These pinch points do not occur in homogenous cases since the reduction in permeability is distributed throughout the fracture network thus, the permeability reduction is not as extreme in the low conductivity branches of the fracture network as it is for heterogeneous cases.
- The difference in cumulative production between homogenously and heterogeneously damaged cases ranged from 10% to 80% increasing with intensity of permeability damage, lower damaged permeability leading to a higher difference in percentage difference. This suggests accounting for proppant damage heterogeneity will be important for accurate prediction results.

Capillary Pressure in Damaged Hydraulic Fracture Networks

Capillary pressure values were determined from empirical data provided in Mattax et al. (1975) and correlated with permeability using the Leverett J function. Heterogeneity in damage was based on the aperture of the hydraulic fracture with fracture branches with lower apertures more likely to be damaged. Simulation cases were run with and without capillary pressure in the damaged hydraulic fractures. Simulations were run over a range of permeability damage from 10% to 90% and later for a range of pressure drawdowns from 100 psi to 3500 psi. Conclusions from the simulation runs are as follows:

- Capillary pressure in the fractures prevents water from draining out of the damaged fractures, reducing gas permeability thus both the cumulative gas and water production over 3 years was higher for cases without capillary pressure then for cases with capillary pressure.
- For cases where damage was homogenous, it was noted that permeability decrease due to damage had a larger effect on gas production than capillary pressure. As permeability damage increased, the pdifference in cumulative gas production between cases with and without capillary pressure decreased.
- As permeability damage increased, unlike homogenously damaged case, percentage difference in cumulative gas production between cases with and without capillary pressure increased.
- The percentage difference in cumulative production over the entire range of permeability damage at a drawdown of 2600 psi did not exceed 3%. Thus it can be concluded that at this bottom-hole pressure, discounting capillary pressure

arising due to gel damage will not have a significant impact on the accuracy of production forecast.

- For simulations run over a range of pressure drawdowns, the percentage difference in cumulative production between cases with and without capillary pressures ranged from 1% at a drawdown of 500 psi to 7% at a drawdown of 3500 psi. Thus at pressure drawdowns at which shale wells are usually produced (2000 psi-3000 psi), ignoring capillary pressure in damaged parts of the hydraulic fracture will not lead to any significant inaccuracy in production forecasting. however, in circumstances where reservoir or well bore limitations force operators to produce at a lower drawdowns, not accounting for capillary pressure might lead to significant error in production forecasting.

5.2 SUGGESTIONS FOR FUTURE WORK

- The simulations conducted in our study were all done without considering the effect of adsorption and non-Darcy flow. If adsorption and non-Darcy flow of gas can be incorporated into the simulations, it would help increase the accuracy of the results.
- Currently, fracture propagation in JOINTS is driven by uniform pressure, not accounting for fluid flow in the fractures and not allowing variable propagation length as a function of volume pumped. Recent work by Wu and Olson (2013) has relieved this shortcoming which could be incorporated into future projects.

- Site specific stress information was not available for this location in the Marcellus hence generic values were assumed. Knowing more about the differential stress (S_{hmax}-S_{hmin}) would greatly increase the accuracy of the fracture propagation simulations.
- Khan (2013) evaluated the effect of fracture network geometry on production response from shale oil reservoirs. However, the fracture networks were artificially created without using a fracture simulator. The workflow presented in this thesis preserves hydraulic fracture complexity; thus it can be a very useful tool in the future to evaluate the effects of fracture geometry and complexity on reservoir response during production and well testing.
- While investigating residual gel damage in hydraulic fractures, we calculated capillary pressures for damaged proppants using Leverett J function values for loose sand from literature. Determining capillary pressure values directly from damaged proppant packs experimentally in a lab would lead to more accuracy in results.

Appendix

This section provides an overview of the keywords used in building the simulation model. Statements in green are comments and explanation and are not part of the actual code.

ECHO
GRIDUNIT (Specifies Units for grid data)
'FEET' /
MAPAXES (Grid Axes with respect to Map coordinates. 0 most of the times)
0 0 0 0 0 0 /
DX (Size of grid block in x-direction. Each value represents each grid block.)
6.56 6.56 6.56 . . . ./
DY (Size of grid block in y-direction)
6.56 6.56 6.56 . . . ./
DZ (Size of grid block in y-direction)
55 55 55 . . . ./
TOPS (Depth of the top of each grid block, starting with the top most layer)
7000 7000 7000 . . . . . .
7055 7055 7055 . . . . . .
7110 7110 7110 . . . . . /

File GPRO
PERMI (Specifies Permeability of each grid block in x-direction)
1e-005 1e-005 1e-005 1e-005. . . . . ./
PERMJ (Specifies Permeability of each grid block in y-direction)
1e-005 1e-005 1e-005 1e-005. . . . . ./
PERMK (Specifies Permeability of each grid block in z-direction)
1e-006 1e-006 1e-006 1e-006. . . . . ./
(Permeblaiites can also be copied, e.g., PERMJ copied from PERMI)
COPY
PERMI PERMJ /
/
(And/or multiplied with factors)
MULTIPLY
PERMK 0.1 /
/

PORO (Specifies Porosity of each grid block)
0.033 0.033 0.033 0.033. . . . ./

INIT File

SWAT (Water Saturation for each grid block)
0.15 0.15 0.15 0.15 0.15. . . . . ./
PRESSURE (Reservoir Pressure for each grid block)
4156 4156 4156 4156 4156 . . . . . ./

PVT file

ECHO
PVTW (Water PVT Properties)
14.7 1 1e-006 1
0
(Reference Pressure B_w Water Compressibility (psi^{-1}) Water Viscosity (cP) Water viscosibility)
/
PVGZ (Dry Gas PVT properties)
130 (Dry gas temperature in Fahrenheit)
/
(Pressure (psia) z-factor Viscosity (CP))
100 0.988759293 0.012548021
200 0.976915604 0.012548046
. . .
. . .
5400 1.01806827 0.012550212
/
DENSITY (Fluid densities at surface conditions in lb./gal)
54 64 0.044
(Oil Water Gas)
/
ECHO
ROCK (Rock Properties)
4000 1e-005
(Reference Pressure (psi) Compressibility (psi^{-1}))

File SCAL

ECHO
SWFN (Water Saturation Functions)
Water Saturation Function for region 1, in this case, matrix
Sw Krw Pc
0 0 550
.1 0 550
. . .
. . .

```
   1          1          10
/
 Water Saturation Function for region 2, in this case, fracture
Sw         Krw       Pc
 0          0          0
 .1         0          0
   .         .          .
   .         .          .
   1         1          0
/
SGFN (Gas Saturation Functions)
Gas Saturation Function for region 1 or matrix
Sg         Krg       Pc
 0          0              0
 .1         0.01           0
   .         .              .
   .         .              .
   1         1              0
/
 Gas Saturation Function for region 2, or fracture
Sg         Krg       Pc
 0          0              0
 .1         0.01           0
   .         .              .
   .         .              .
   1         1              0
/
```

SCH File

```
ECHO
 WELSPECS (Well specifications)
'PROD1' 'P' 30 81 1* 'GAS' 1* 'STD' 'SHUT' 'YES' 1* 'SEG' 3* 'STD' /
Well Name, Group, I Location, J Location, Datum Depth, Preferred Phase, Drainage
Radius, Inflow Equation, Automatic Shut-in Instruction, Cross flow, PVT property Table,
Density Calculation
/
RPTSCHED
0  0  0  0  0  0  2  2  2  1  0  2  0  1  0  0  0
0  0  0  0  0  0  0  0  0  0  0  0  0  0  2  0  0
0  0  0  0  0  0  0  0  0  0  0  0  0  0  0  0  /
COMPDAT (Well completion specifications)
'PROD1' 30 81 2 2 'OPEN' 2* 0.325 3* 'Y' 1* /
(Name, I Location, J Location, K location for the top of perforations, K location for the
bottom of perforations, Completions open or close, Saturation table for connected relative
```

permablities, Well radius, Effective Kh for the connection, Direction in which well penetrates the grid block, Pressure equivalent radius)
/

COMPDAT
'PROD1' 31 81 2 2 'OPEN' 2* 0.325 3* 'Y' 1* /
/
COMPDAT
'PROD1' 32 81 2 2 'OPEN' 2* 0.325 3* 'Y' 1* /
.
.
.
.
.
COMPDAT
'PROD1' 824 81 2 2 'OPEN' 2* 0.325 3* 'Y' 1* /
/
Multiple COMPDAT keywords, with varying J location were used to specify a horizontal well.
WCONPROD (Well Production controls)
'PROD1' 'OPEN' 'BHP' 1e+020 1e+020 1e+020 1e+020 1e+020 1100 3* 6* 1* /
(Name, Open/shut status, Control, Oil rate, Water rate, Gas rate, Liquid rate, Reservoir Volume rate, BHP Target,)
TSTEP (Time step in days)
7 /
WCONPROD
'PROD1' 'OPEN' 'BHP' 1e+020 1e+020 1e+020 1e+020 1e+020 1200 3* 6* 1* /
The above sequence of keywords, changes the bottom hole pressure from 1100 psi to 1200 psi after 7 days of production.

References

Agarwal, R. G., Carter, R. D., & Pollock, C. B. (1979, March 1). Evaluation and Performance Prediction of Low-Permeability Gas Wells Stimulated by Massive Hydraulic Fracturing. Society of Petroleum Engineers. doi:10.2118/6838-PA

Ajayi, B. T., Walker, K. J., Wutherich, K., & Sink, J. (2011, January 1). Channel Hydraulic Fracturing and Its Applicability in the Marcellus Shale. Society of Petroleum Engineers. doi:10.2118/149426-MS

Almond, S. W., Bland, W. E., & Ripley, H. E. (1984, January 1). The Effect Of Break Mechanisms On Gelling Agent Residue And Flow Impairment In 20/40 Mesh Sand. Petroleum Society of Canada. doi:10.2118/84-35-30

Barree, R. D., Cox, S. A., Barree, V. L., & Conway, M. W. (2003, January 1). Realistic Assessment of Proppant Pack Conductivity for Material Selection. Society of Petroleum Engineers. doi:10.2118/84306-MS

Bostrom, B. (2009, January 1). Development of a Geomechanical Reservoir Modelling Workflow and Simulations. Society of Petroleum Engineers. doi:10.2118/124307-MS

Charoenwongsa, S., Kazemi, H., Fakcharoenphol, P., & Miskimins, J. L. (2012, January 1). Simulation of Gel Filter Cake Formation, Gel Cleanup, and Post-Frac Well Performance in Hydraulically Fractured Gas Wells. Society of Petroleum Engineers. doi:10.2118/150104-MS

Cheng, Y. (2012, March 1). Impact of Water Dynamics in Fractures on the Performance of Hydraulically Fractured Wells in Gas-Shale Reservoirs. Society of Petroleum Engineers. doi:10.2118/127863-PA

Christiansen, R.L. 2001. *Two-Phase Flow through Porous Media*, Ch. 1, 4, and 5. Littleton, Colorado: KNQ Engineering.

Cipolla, C. L. (2009, September 1). Modeling Production and Evaluating Fracture Performance in Unconventional Gas Reservoirs. Society of Petroleum Engineers. doi:10.2118/118536-JPT

Cohen, C.-E., Xu, W., Weng, X., & Tardy, P. M. J. (2012, January 1). Production Forecast after Hydraulic Fracturing in Naturally Fractured Reservoirs: Coupling a Complex Fracturing Simulator and a Semi-Analytical Production Model. Society of Petroleum Engineers. doi:10.2118/152541-MS

Cooke, C. E. (1975, October 1). Effect of Fracturing Fluids on Fracture Conductivity. Society of Petroleum Engineers. doi:10.2118/5114-PA

Dean, R. H., & Schmidt, J. H. (2008, January 1). Hydraulic Fracture Predictions With a Fully Coupled Geomechanical Reservoir Simulator. Society of Petroleum Engineers. doi:10.2118/116470-MS

Devegowda, D., Sigal, R., Civan, F. and Andrade, J. 2010. Issues with the Simulation of Shale Gas Reservoirs. Paper presented at the AAPG/SPE/SEG Hedberg Conference, Austin, TX, Dec 5-10.

"ECLIPSE Industry Reference Reservoir Simulator." *ECLIPSE Industry Reference Reservoir Simulator*. Schlumberger, n.d. Web. <http://www.software.slb.com/products/foundation/Pages/eclipse.aspx>.

Engelder, T., Lash, G.G., and Uzcategui, R.S. 2009. Joint Sets That Enhance Production from Middle and Upper Devonian Gas Shales of the Appalachian Basin. AAPG Bulletin 93: 857.

Fisher, M. K., Wright, C. A., Davidson, B. M., Goodwin, A. K., Fielder, E. O., Buckler, W. S., & Steinsberger, N. P. (2002, January 1). Integrating Fracture Mapping Technologies to Optimize Stimulations in the Barnett Shale. Society of Petroleum Engineers. doi:10.2118/77441-MS

Gale, J.F.W., Reed, R.M., and Holder, J. 2007. Natural Fractures in the Barnett Shale and Their Importance for Hydraulic Fracture Treatments. AAPG Bulletin 91: 603

Gale, J. F. W., Pommer, L., Laubach, S. E., Olson.J.,Holder.J., Naseem.K., (2012, August 8). Marcellus Shale BEG Natural Fracture Project Final Report.

Gel Damage. CARBO Ceramics, n.d. Web. <http://pwaa000102.psiweb.com/English/tools/topical_ref/tr_gel.html>

Gomez, L.A., 2007, Characterization of the Spatial Arrangement of Opening-Mode Fractures. Ph.D. Dissertation, UT Austin.

Holditch, S. A. (1979, December 1). Factors Affecting Water Blocking and Gas Flow From Hydraulically Fractured Gas Wells. Society of Petroleum Engineers. doi:10.2118/7561-PA

Hubbert, M.K. and Willis, D.G., 1957, Mechanics of hydraulic fracturing. Transactions of American Institute of Mining Engineering, 210, 153-168.

Jacot, R. H., Bazan, L. W., & Meyer, B. R. (2010, January 1). Technology Integration: A Methodology To Enhance Production and Maximize Economics in Horizontal Marcellus Shale Wells. Society of Petroleum Engineers. doi:10.2118/135262-MS

Khan, A. M. (2013). Multi-frac treatments in tight oil and shale gas reservoirs: effect of hydraulic fracture geometry on production and rate transient (MS thesis). University of Texas, Austin, TX.

Leverett, M. C. (1941, December 1). Capillary Behavior in Porous Solids. Society of Petroleum Engineers. doi:10.2118/941152-G

Li, J., Du, C., & Zhang, X. (2011, January 1). Critical Evaluations of Shale Gas Reservoir Simulation Approaches: Single Porosity and Dual Porosity Modeling. Society of Petroleum Engineers. doi:10.2118/141756-MS

Mattax, C. C., McKinley, R. M., & Clothier, A. T. (1975, December 1). Core Analysis of Unconsolidated and Friable Sands. Society of Petroleum Engineers. doi:10.2118/4986-PA

Marrett, R.A., Gale, J.F.W. and Gomez, L.A., 2005, Spatial Arrangement of Fractures III −Correlation Analyses. Unpublished report prepared for University of Texas Fracture Research and Application Consortium.

Marrett R., Laubach S.E. and Olson J.E. 2007. Anisotropy and beyond: Geologic perspectives on geophysical prospecting for natural fractures. The Leading Edge 26, 1106–1111.

Mayerhofer, M. J., Lolon, E. P., Youngblood, J. E., & Heinze, J. R. (2006, January 1). Integration of Microseismic-Fracture-Mapping Results With Numerical Fracture Network Production Modeling in the Barnett Shale. Society of Petroleum Engineers. doi:10.2118/102103-MS

Mayerhofer, M. J., Lolon, E., Warpinski, N. R., Cipolla, C. L., Walser, D. W., & Rightmire, C. M. (2008, January 1). What is Stimulated Rock Volume? Society of Petroleum Engineers. doi:10.2118/119890-MS

Mayerhofer, M. J., Stegent, N. A., Barth, J. O., & Ryan, K. M. (2011, January 1). Integrating Fracture Diagnostics and Engineering Data in the Marcellus Shale. Society of Petroleum Engineers. doi:10.2118/145463-MS

Mirzaei, M., & Cipolla, C. L. (2012, January 1). A Workflow for Modeling and Simulation of Hydraulic Fractures in Unconventional Gas Reservoirs. Society of Petroleum Engineers. doi:10.2118/153022-MS

Nassir, M., Settari, A., & Wan, R. G. (2014, March 1). Prediction of Stimulated Reservoir Volume and Optimization of Fracturing in Tight Gas and Shale With a Fully Elasto-Plastic Coupled Geomechanical Model. Society of Petroleum Engineers. doi:10.2118/163814-PA

Olson, J. E. (2008, January 1). Multi-fracture propagation modeling: Applications to hydraulic fracturing in shales and tight gas sands. American Rock Mechanics Association.

Palisch, T. T., Duenckel, R. J., Bazan, L. W., Heidt, J. H., & Turk, G. A. (2007, January 1). Determining Realistic Fracture Conductivity and Understanding its Impact on

Well Performance - Theory and Field Examples. Society of Petroleum Engineers. doi:10.2118/106301-MS

Penny, G. S., Crafton, J. W., Champagne, L. M., & Zelenev, A. S. (2012, January 1). Proppant and Fluid Selection To Optimize Performance of Horizontal Shale Fracs. Society of Petroleum Engineers. doi:10.2118/152119-MS

Reese, J. L. (2007). Simulating Gas Production from Hydraulic Fracture Networks: A Case study of Barnett Shale (MS thesis). University of Texas, Austin, TX.

Settari, A., & Mourits, F. M. (1998, September 1). A Coupled Reservoir and Geomechanical Simulation System. Society of Petroleum Engineers. doi:10.2118/50939-PA

Starr, J. (2011, January 1). Closure Stress Gradient Estimation of the Marcellus Shale From Seismic Data. Society of Exploration Geophysicists.

Williams-Stroud, S. C., Neuhaus, C. W., Telker, C., Remington, C., Barker, W., Neshyba, G., & Blair, K. (2012, January 1). Temporal Evolution of Stress States From Hydraulic Fracturing Source Mechanisms in the Marcellus Shale. Society of Petroleum Engineers. doi:10.2118/162786-MS

Wang, J. Y., Holditch, S. A., & McVay, D. (2009, January 1). Modeling Fracture Fluid Cleanup in Tight Gas Wells. Society of Petroleum Engineers. doi:10.2118/119624-MS

Wang, Q., Guo, B., & Gao, D. (2012, January 1). Is Formation Damage an Issue in Shale Gas Development? Society of Petroleum Engineers. doi:10.2118/149623-MS

Warpinski, N. R., Mayerhofer, M. J., Vincent, M. C., Cipolla, C. L., & Lolon, E. (2008, January 1). Stimulating Unconventional Reservoirs: Maximizing Network Growth While Optimizing Fracture Conductivity. Society of Petroleum Engineers. doi:10.2118/114173-MS

Wattenbarger, R. A., El-Banbi, A. H., Villegas, M. E., & Maggard, J. B. (1998, January 1). Production Analysis of Linear Flow Into Fractured Tight Gas Wells. Society of Petroleum Engineers. doi:10.2118/39931-MS

Weng, X., Kresse, O., Cohen, C. E., Wu, R., & Gu, H. (2011, January 1). Modeling of Hydraulic Fracture Network Propagation in a Naturally Fractured Formation. Society of Petroleum Engineers. doi:10.2118/140253-MS

Williams-Stroud, S. C., Neuhaus, C. W., Telker, C., Remington, C., Barker, W., Neshyba, G., & Blair, K. (2012, January 1). Temporal Evolution of Stress States From Hydraulic Fracturing Source Mechanisms in the Marcellus Shale. Society of Petroleum Engineers. doi:10.2118/162786-MS

Xu, W., Thiercelin, M. J., Ganguly, U., Weng, X., Gu, H., Onda, H., … Le Calvez, J. (2010, January 1). Wiremesh: A Novel Shale Fracturing Simulator. Society of Petroleum Engineers. doi:10.2118/132218-MS

Zhang, X., Du, C., Deimbacher, F., Crick, M., & Harikesavanallur, A. (2009, January 1). Sensitivity Studies of Horizontal Wells with Hydraulic Fractures in Shale Gas Reservoirs. International Petroleum Technology Conference. doi:10.2523/13338-MS